Materials Horizons

ROYAL SOCIETY OF CHEMISTRY

REVIEW

View Article Online
View Journal | View Issue

Cite this: *Mater. Horiz.*, 2022, **9**, 1825

Advances in 4D printing of liquid crystalline elastomers: materials, techniques, and applications

Zhecun Guan,[a] Ling Wang *[b] and Jinhye Bae *[acd]

Liquid crystalline elastomers (LCEs) are polymer networks exhibiting anisotropic liquid crystallinity while maintaining elastomeric properties. Owing to diverse polymeric forms and self-alignment molecular behaviors, LCEs have fascinated state-of-the-art efforts in various disciplines other than the traditional low-molar-mass display market. By patterning order to structures, LCEs demonstrate reversible high-speed and large-scale actuations in response to external stimuli, allowing for close integration with 4D printing and architectures of digital devices, which is scarcely observed in homogeneous soft polymer networks. In this review, we collect recent advances in 4D printing of LCEs, with emphases on synthesis and processing methods that enable microscopic changes in the molecular orientation and hence macroscopic changes in the properties of end-use objects. Promising potentials of printed complexes include fields of soft robotics, optics, and biomedical devices. Within this scope, we elucidate the relationships among external stimuli, tailorable morphologies in mesophases of liquid crystals, and programmable topological configurations of printed parts. Lastly, perspectives and potential challenges facing 4D printing of LCEs are discussed.

Received 24th February 2022,
Accepted 22nd April 2022

DOI: 10.1039/d2mh00232a

rsc.li/materials-horizons

[a] *Department of Nanoengineering, University of California San Diego, La Jolla, CA 92093, USA. E-mail: j3bae@ucsd.edu*
[b] *School of Materials Science and Engineering, Tianjin University, Tianjin 300350, P. R. China. E-mail: lwang@tju.edu.cn*
[c] *Chemical Engineering Program, University of California San Diego, La Jolla, CA 92093, USA*
[d] *Materials Science and Engineering Program, University of California San Diego, La Jolla, CA 92093, USA*

Zhecun Guan

Zhecun Guan is a PhD student in NanoEngineering under the supervision of Prof. Jinhye Bae. Her research interests lie in the development of stimuli-responsive polymers as well as processing methods for 3D printing. She studied at China University of Geosciences (CUG) in China and obtained her bachelor's degree in 2020. She did a research visit at Tianjin University as a 1st year PhD student, then started working as a graduate student researcher at the University of California San Diego, USA.

Ling Wang

Ling Wang is a professor at the School of Materials Science and Engineering of Tianjin University. He received his PhD degree of Materials Science from the University of Science and Technology Beijing in 2013. He worked as a Postdoctoral Research Fellow and Senior Research Fellow at the Advanced Materials and Liquid Crystal Institute of Kent State University, and Texas A&M University, respectively. His research interests are design, synthesis, and properties of smart soft materials, bioinspired materials, and functional nanomaterials, and their emerging applications in diverse fields ranging from soft robotics, adaptive camouflage, and additive manufacturing to energy and safety issues.

1. Introduction

Nature is an everlasting source to inspire the advancement of smart materials that can respond and adapt to environmental changes. One well-known example is the Venus flytrap, whose leaves autonomously close upon mechanical stimulation on a sub-second scale.[1] Similarly, pinecones are capable of opening or closing their scales in response to ambient humidity, owing to two kinds of tissues with cellulose fibrils of different directions that generate anisotropic absorption/desorption of water.[2] Despite adaptive characteristics in the botanical world, stimuli-responsiveness can be ubiquitously found among a variety of animals. For instance, the skin of cephalopods contains numerous chromatophores and structural reflectors which manipulate the reflected light through muscle contraction and expansion, thus enabling adaptive camouflage to avoid predators.[3] The complexity, intelligence, and sophistication of stimuli processing in living creatures have triggered mimicry and exploitation of these physiological features to deployable devices. To date, the mainstream research on artificial intelligence that mimics organisms is based on computer programming, and the range-of-use is restricted to remote-controlled electronic systems.[4] However, the evolution of integrated computing circuitry, power sources, and electrically driven actuators, occurring primarily through combination, requires a relatively large-scale body with rigid mechanical arms. This impedes the development of a miniaturized robotic system that can noninvasively access highly confined spaces.[5,6]

With the increasing demand for flexibility, controllability, and intelligence of structural building blocks in both academia and industry, rigid materials are no longer applicable for a wide range of such applications. In a reverse manner to stiff materials, though in their early stage, soft biomimetic robotics has shown tangible benefits in human–machine interaction and adaptability to wearable devices.[7,8] Notably, soft matter-based freestanding stimuli-responsive structures, which could be stimulated and actuated autonomously by untethered power sources, have witnessed the development of next-generation actuators. To efficiently extract and transfer energy to steady mechanical work, an extensive array of stimuli-responsive materials have been investigated to actuate shape-shifting behaviors. Shape memory polymers (SMPs), hydrogels, and liquid crystal elastomers (LCEs) are the three mostly explored categories of smart soft matter, owing to their non-equilibrium matter transport or phase transition upon stimulation.[9] Specifically, a typical SMP can be programmed to fix one temporary configuration and subsequently recover to its permanent shape under external stimuli (typically heating).[10] Here, the temporary shape is usually programmed by applying force during the shape fixing step. Unless reprogramming, the irreversible actuation blocks SMPs from instant shape morphing, which tremendously increases instability manufacturing.[11,12] For example, thermomechanical programming of thermo-responsive SMPs begins with heating and mechanical loading, while requires cooling process and unloading prior to actual deployment or actuation.[13] Polymeric hydrogels are a group of biomimetic soft materials composed of crosslinked hydrophilic networks that undergo large volume changes by water absorption or desorption, representing an important class of stimuli-responsive materials.[14–16] Unlike SMPs, thermo-responsive hydrogels with lower critical solution temperature (LCST) can be reversibly hydrated and dehydrated below and above the LCST, respectively.[17] It should be noted that poly(*N*-isopropylacrylamide) (PNIPAM) is one of the most common thermo-responsive hydrogels, which experiences a volume shrinkage of about 90% when transferred from a hydrophilic to a hydrophobic state.[18,19] Besides large deformation upon temperature change, hydrogels generally possess excellent biocompatibility for biomedical applications due to high water content.[20–22] Meanwhile, the inherent softness of hydrogels and diffusion-driven shape-morphing mechanism result in relatively low responsive speed, severely hindering the rapid and complete development of large-scale geometries.[23,24] LCEs are another category of stimuli-responsive materials with two-way actuation behavior under various stimuli including heat,[25] light,[26,27] electric,[28] and magnetic fields.[29] With the phase transition between nematic and isotropic phases at the nematic–isotropic temperature (T_{NI}), microscopic domain rearrangements elicit reversible and anisotropic shape contraction or elongation. Upon heating above T_{NI}, for instance, the aligned liquid crystal mesogenic units lose their original orientation and become randomly arranged.[30,31] The high strain response can be obtained by regulating mesophase within LCEs, which prepares LCEs as fascinating candidates for smart actuators and other emerging applications in biomedical and optical fields.[32–35] In general, the oligomerization process as the last step in LCE synthesis generates polydomain liquid crystalline products, so post-treatments to align mesogens into monodomains are required to initiate a strain response by stimuli. Several approaches have been introduced to realize mesogenic alignments, including surface rubbing,[36] electrical and magnetic fields,[37] polarized light,[38,39] evaporation,[40] and mechanical stretching.[41] However, most of these methods are applied in a lamellar manner, thus impeding the three-dimensional arrangement of mesogens and the realization of LCEs with desired morphologies.[42] As a result, thin films are the main

Jinhye Bae

Jinhye Bae is an assistant professor in the Department of Nano-Engineering at the University of California San Diego. She received her PhD in Polymer Science and Engineering at the University of Massachusetts Amherst in 2015, then worked in the School of Engineering and Applied Sciences at Harvard University as a postdoctoral fellow. Her research focuses on understanding the physical and chemical properties of polymeric materials to program their shape reconfiguration and responsiveness. Her research interests also include the integration of material characteristics into new structural design and fabrication approaches for applications in biomedical devices, soft robotics, actuators, and sensors.

components of LCE structures which simply form aligned mesophases within liquid crystal cells.

Despite decades of efforts paid to LCEs, their potentials have not been magnified until the combination of new chemistries that overcome barriers to LCE synthesis and the recent advent of 4D printing.[43] Invented in 1986, 3D printing refers to a process of joining materials together to make customer-designed 3D objects without the use of models.[44] The burgeon of 3D printing technology has allowed us to fabricate more complex geometries than films and laminar structures. Diverse materials could be employed to print desired structures, including metals, ceramics, polymers, and other composites.[45] As 3D printing has demonstrated precision and versatility in stereo setups, this area has made intense efforts in both scientific advances and industrial scale-up.[46,47] In 2013, Tibbits first raised the concept of "4D printing" and introduced time as the additional fourth dimension, extending time-dependent changes to printing systems.[48] Specifically, 4D printing is the optimization of 3D printed structures with time-evolving mechanical properties in shape, functionality, and dimension. This term has recently been correlated to 3D-printed soft intelligence in a predetermined manner in response to stimuli such as temperature,[49] light irradiation,[50] magnetic fields,[51] humidity,[52] electricity,[53] and chemicals.[54] With the synchronous processes to achieve mesogenic alignments while building up complex structures, 4D printing opens new avenues for liquid crystalline materials by enabling a more comprehensive toolbox for controllable shape programming.[55]

4D printing of LCEs has witnessed a rapid growth in the number of publications and citations in the past five years from 2017 to 2021, searching by the topics of 4D printing and 3D printing of LCEs from Web of Science. It is worth noting that the number of citations increases more dramatically than the publications (Fig. 1a). Five methodologies have been reported to facilitate 4D printing of LCE since the first occurrence in 2017, including direct ink writing (DIW),[56] fused deposition modeling (FDM),[57] stereolithography (SLA),[58] digital light processing (DLP),[59] and inkjet printing.[60] Holding 55% of the total publications by summation of the five printing techniques, extrusion-based DIW has been the most extensively utilized method, with DLP and inkjet printing following behind (Fig. 1b). Vat photopolymerization-based methods that selectively cure structures from a prefilled vat, including DLP and SLA, also account for a large percentage of all publications on this topic. Over the past years, several review articles have discussed the history and development of 3D to 4D printing from diverse perspectives.[44,56,61–64] For example, Momeni *et al.* introduced the 4D printing process and summarized the practical concepts and related tools.[43] Spiegel *et al.* addressed both the potential and challenges of micro-structural material design and performances when utilizing 4D printing.[63] This review discusses the state-of-the-art account of 4D printing facilitated LCE structures. The ink chemistry of LCEs, printing techniques and parameters, properties of printed structures, as well as external stimuli-induced complexity of the shape-morphing process are discussed. Most recently, del Pozo *et al.* provided a didactical overview of the crossover field of the liquid crystal-additive manufacturing junction.[65] Based on the resolution mostly achieved, the processing methods and liquid crystal products are classified into micrometer-scale and millimeter-scale. From a different perspective, we highlight the intrinsic temperature-responsive rearrangement of mesophases at T_{NI} and how each printing method manages to monitor the molecular alignment of LCEs. The prospects of 4D printed LCEs in the fields of smart soft robotics and emerging applications have been summarized, such as rolling robots,[66] self-propelling structures,[67] braille,[68] adaptive lens,[69] substrates for cell culture and implantation (Fig. 2).[70,71] For each application scenario, we discuss in detail a few rationally designed and developed devices for creating material systems. Finally, we conclude with insights to the development and barriers in 4D printing systems of the reconfigurable and programmable LCEs, thus inspiring new strategies to overcome the current

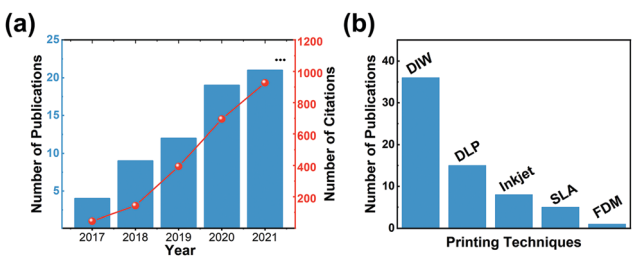

Fig. 1 The statistics data of publication on the topic of 4D printing and 3D printing of LCEs from Web of Science: (a) publications and citations in each year, and (b) publications for 3D printing using different printing techniques. Data were collected in the past 5 years (2017 to 2021).

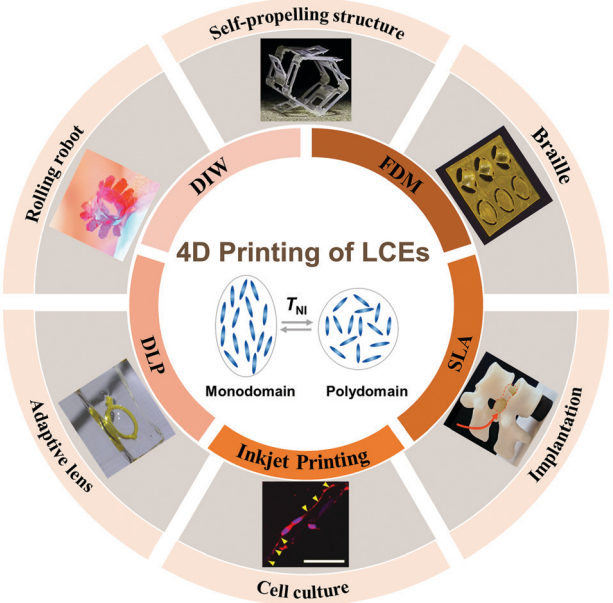

Fig. 2 Representative mechanism, printing methods (DIW, FDM, SLA, DLP, and inkjet printing), and applications of 4D printing of LCEs. (*e.g.*, rolling robot, self-propelling structure, braille, adaptive lens, bone implantations and cell culture.) Reproduced with permission.[66–71] Copyrights 2018, 2019, 2020, 2020, 2020, Wiley-VCH, Copyright 2019, American Association for the Advancement of Science.

limitations and move towards their practical applications in the areas of soft robotics, biomedical science, optics, and many other soft intelligence.

2. Chemistry and alignment of LCEs

Liquid crystal (LC) refers to a state of matter between a crystalline solid and an isotropic liquid, in which self-organize to long-range orientational or positional order at the molecular level.[58,72–74] Thermotropic and lyotropic LCs are usually classified based on the mechanism of formation.[41] In thermotropic LCs, the LC phases occur as a function of temperature variation. Compounds of rod-like (also known as calamitic), disc-like (also known as discotic), and bent-core anisotropic geometries are capable of exhibiting thermotropic LC phases.[75] The phase transition of lyotropic LCs depends on both temperature and mesogenic concentration. Basically, the spontaneous organization could be attributed to the mesogens, the main composition of LCs with elongated, stiff rod-like molecules. The rigid backbone of single mesogens comprises aromatic rings and double bonds along the long axis, while the flexible ends endow mesogens with the capability to reorient smoothly. Physical properties, such as temperature, birefringence, and dielectric properties, are severely influenced by the structure of aromatic rings.[76]

With a suitable ambient temperature, mesogens undergo self-organization into a nematic phase (N); some can form smectic phases (S_m, including smectic A and smectic C phases) in both orientational and spatial order with longer flexible units.[77,78] The orientation among mesogens is interrupted upon an elevated temperature, and the phase transformation between nematic and isotropic phases leads to microscopic domain rearrangements as well as macroscopic shape transformation. The arrangement of mesogens within LCs is also known as the director field. The molecular director, denoted as $\hat{n}$, refers to the spatial and temporal average symmetry of the long axis of rod-like mesogens. Order parameter (S) is also called as Hermans–Stein orientation factor, which can be expressed by the function of angle (θ) between mesogens and local director, quantitatively measuring the uniaxial orientation of crystalline polymers.[79] As the order parameter could be evaluated through wide-angle X-ray scattering (WAXS, eqn (1)), they have been widely employed to determine the anisotropy degree of mesogens.[80]

$$S = 1 - N^{-1} \times \frac{3}{2}\int_0^{\pi/2} /(\theta)\left[\sin^2\theta + (\sin\theta\cos^2\theta)\log\frac{1+\sin\theta}{\cos\theta}\right]\mathrm{d}\theta \quad (1)$$

where $N = \int_0^{\pi/2} /(\theta)\mathrm{d}\theta$.

Efforts paid in exploiting the phase transition of LCs have never remitted since the first witness of this phenomenon over 150 years ago.[81] The flourishment of low-molar-mass LCs has significantly advanced display technologies and revealed capacities in areas such as energy-harvesting devices,[82] mechanical actuators,[83] wearable sensors,[84–86] and novel films in past centuries.[87,88] In 1975, de Gennes and Seances first recognized the interplay between the LC phase and the macromolecular network architecture, which generates exceptional physical properties that resemble hierarchies in muscle structures and other biological systems.[89,90] Inspired by their prospective work, various polymers showing liquid crystallinity have been investigated in controlling polymer networks and liquid crystallinity simultaneously. These polymeric materials have been related by a variety of names, such as liquid crystal polymers (LCPs), liquid crystal networks (LCNs), and LCEs. LCPs are uncrosslinked main-chain macromolecules that can organize into LC phases during processing, by which the unique anisotropic performances are retained. LCNs maintain some of the high performances of LCPs, while possessing a moderately crosslinked network that offers flexibility in order change of as much as 5% when exposed to appropriate stimuli.[91] Unlike LCPs or LCNs, LCEs exhibit large order changes and hence dramatic and reversible deformations while responding to stimuli, owing to the flexibility of polymer chain backbones and low overall crosslink density in elastomeric networks.[92] LCEs contain main-chain and side-chain LCEs, which are differentiated by the ways mesogens are connected to polymer backbones. Mesogens in a main-chain LCE are linked together within the polymer through their long axes, while in a side-on side-chain LCE, the mesogens and backbones are connected by a short sparer.[93] In this section, we review the mechanics of LCEs with emphases on preparation, properties, and approaches for controlling alignment, given their predominant roles as ink materials in 4D printing.

2.1 Chemistry of printable LCEs

A variety of preparation strategies, subcategorized into two selections by starting materials, have been developed to obtain the LC state in an elastomeric network over the past decades. H. Finkelmann *et al.* summarized the principles and differences of LCE synthesis between starting with all monomers and beginning with a linear LC polymer with known LC phase behaviors.[90] For the synthesis as well as for the usability of the networks the transition temperatures are the most important factors as they determine the regime of use and hence the functionality of the LC structure. These are the LC phase-to-isotropic phase transition temperature ($T_{LC,I}$, mostly nematic-to-isotropic phase temperature T_{NI}) and the glass transition temperature (T_g) wherein the transfer from glassy states to LC states happens. T_{NI} can be adjusted within the desired range for maximized physical properties by manipulating the structures of monomers and the main chain. Moreover, T_{NI} can be systematically modified by copolymerization with different mesogenic or non-mesogenic co-monomers. In the case of glass transition, T_g functions as an indicator of the flexibility of LCEs and can be determined by the flexibility of the main chain, the interaction between mesogens, the interaction between the main chain and mesogens, and crosslinking densities. The transformation from a LC phase to a crystalline phase at $T_{Cry,LC}$ (T_{CryN}) can hardly achieve, given the complex structure of LCEs and possible network damage.

Two main methods have been utilized in side-chain elastomers synthesis: radical polymerization and hydrosilylation polymerization. Radical polymerization begins with light- or heat-induced radicals, then unsaturated double bonds in acrylates or methacrylates are attacked and disrupted, which interact with adjacent double bonds until full polymerization. A low selectivity of the chemical composition, which allows for various starting materials in this process, results in C–C backbones. Radical polymerization can be carried out in bulk in principle, however, only if the polymerization temperature is within the overlapping temperature regime where monomers and polymers exhibit the same LC phase a homogeneous reaction can take place. Otherwise, the de-mixing occurs, which causes an uncontrolled network formation. Furthermore, the large reaction enthalpy of the polymerization restricts this method to the preparation of thin films only, in which suitable heat transfer and control are guaranteed. Due to the high chain anisotropy, the hydrosilylation process is the most commonly used method in synthesizing side-chain elastomers, with larger actuation and lower T_g.[94] Hydrosilylation polymerization employs Si–H bonds to connect with unsaturated C═O and C═C bonds and hence complete the valence structure of the carbon atom. In addition, this reaction allows for multi-step polymerization. For example, when vinyl and methacrylate groups are both introduced to the reaction, vinyl groups quickly form an initial network while methacrylate groups reacted slowly to fully crosslink the matrix. Thus, the mechanical orientation of mesogens, such as stretching, could be achieved in the stepwise polymerization.[95]

Unlike side-chain LCEs, the direct coupling of mesogens and chain conformation of high anisotropy have garnered significant attention for optimized mechanical properties in main-chain LCEs.[96,97] Historically, step-growth reactions are the limited methods for main-chain elastomer preparation, *i.e.*, polycondensation and polyaddition reactions. Most main-chain LCEs show high clearing temperature and tend to crystallize instead of retaining elastomer properties, mainly stemming from the rod-like rigid moieties lying in the main chain of polymers. These chemistries also highly require the purity of starting materials and appropriate reaction conditions to exclude side reactions, thus largely interrupting the realization of scalable main-chain elastomers.[98] Click reactions have always been a fascinating topic as a facile method in synthesizing main-chain LCEs. Although the copper-catalyzed alkyne-azide cycloaddition (CuAAC) was the quintessential click reaction, little work have been done with this mechanism.[99]

Due to the emergence of new chemistries developed these years, commercially available monomers without any further purification process are now commonly applied to the fabrications (Fig. 3a). They are also insensitive to reaction conditions, and some allow a second-stage crosslinking step to be delayed indefinitely. Likewise, Michael addition click reaction has surged to clarify the structure–property relationship in LCEs. The most employed click reactions include photo-initiated thiol–ene Michael addition reaction, nucleophile-catalyzed thiol–acrylate Michael addition reaction, and nucleophile-catalyzed aza-Michael addition reaction, as

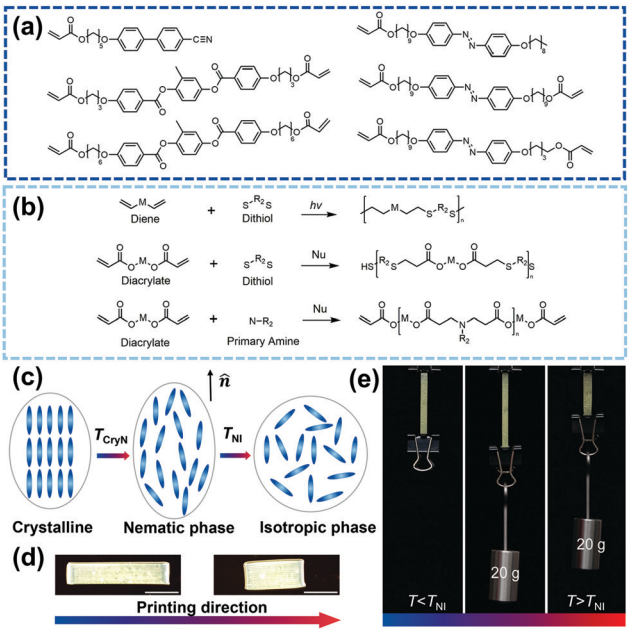

Fig. 3 Preparation and properties of LCEs. (a) Chemical structures of representative LC monomers. (b) Reaction schemes for the various click reactions used to synthesize LCEs. Nucleophile-catalyzed Michael addition click reaction is shown with excess acrylate that allows for a second photopolymerization step. (c–e) Thermo-responsive phase transition and soft elasticity of LCEs. (c) Conformation change when crystalline-to-nematic and nematic-to-isotropic phase transition happens. The repeating units stand for mesogenic moieties of LCs. (d) Images of printed (left) and actuated (right) LCEs fabricated using a unidirectional print path (scale bar = 5 mm). (e) Images of a unidirectional printed LCE strip lifting a 20 g weight at different temperatures. Reproduced with permission.[103] Copyright 2018, Wiley-VCH.

illustrated in Fig. 3b.[41] Radical-initiated thiol–ene Michael addition reaction was first used to create linear LCPs in 1997.[100] The reaction between thiol and ene, such as vinyl or acrylate group, could be activated by the radicals generated from photo- or thermal-initiators. In a different manner from free-radical polymerization, this specific chemistry enables non-carbon groups to be introduced into the polymer backbones. Yang and co-workers first published the main-chain LCEs prepared by photopolymerization using this chemistry, with individual pillars behaving as microactuators, leading to reversible contraction of around 300–400%.[101] However, the preparation of thick and large LCEs is restricted by the attenuation of UV irradiation through the thickness of the sample. To facilitate ink materials to tailorable 3D modeling, enormous efforts have been undertaken to liquid crystalline materials. The sensitivity of the order to stimuli is strongly dependent on the composition of the polymer. A low crosslinking density of LCEs allows for large responses in the inner strain and shape deformation to heat treatment.[102] When the temperature is above or below T_{NI}, LC mesogens exhibit reversible microscopic phase transition and LCEs show macroscopic contraction or elongation (Fig. 3c and d). A single strip of LCE shrinks along the director and expands along the orthogonal directions. Employing such a strip, the actuation strain enabled a weight-lifting roughly 1000 times of their own

weight (106 ± 1.5 mg, Fig. 3e).[103] Fast responsivity and large strains of around 400% endow LCEs with unprecedented potential in shape transformation-based actuators, since their invention in 1981.[104] By introducing more director distributions, complex shape transformation and movements could be realized. These thermo-responsive characteristics show the unique capacities of LCEs for artificial muscles, as the representative of soft robotics and biomedical applications. Catalysts, rather than radicals, have been harnessed in nucleophile-catalyzed Michael addition reaction. The Yakacki research group reported a one-pot thiol–acrylate Michael addition reaction to synthesize polydomain LCEs.[105] White group introduced their advance in amine–acrylate aza-Michael addition reaction almost concurrently.[106] These reactions facilitate the fabrication of bulk LCE samples, with commercially available acrylated mesogens, such as RM 257 and RM 82. Moreover, both chemistries allow for a second photopolymerization step with excess acrylate. Similar to the second part of two-step hydrosilylation, a non-stoichiometric ratio of functional groups would lock-in the alignment of mesogens and produce a permanent monodomain. The remnant reactants allow for self-assembly to patterned surfaces, whereas Finkelmann method requires mechanical stretching to achieve orientation. Utilizing this recipe published by the White research group, *n*-butylamine chain extends RM82 through aza-Michael addition, with Irgacure 651 added to activate the acrylate ending groups. Ren *et al.* designed layered shape-morphing patterns and used catalyst-free ink to print complex geometries *via* printing speed encoding upon UV exposure.[107]

Despite the success in implementing click reactions to realize monodomain LCEs, challenges such as the inability to reprogram and form complex structures still exist. Covalent adaptable networks (CANs) provide a novel strategy to synthesize monodomain LCEs with dynamic covalent bond exchange.[108,109] Traditionally, monodomain LCEs are obtained from external effects including rubbing, polarized light-induced photo-alignment, and the aforementioned two-stage crosslinking.[106,110] When CANs are integrated into LCEs, however, mesogens could be manipulated by post-polymerization under certain stimuli. Most of the monodomain LCEs with exchangeable links were prepared based on transesterification,[111,112] transcarbamoyalation,[113] disulfide,[114–116] and allyl sulfide groups.[117–119] The self-healing ability and reset of programmed monodomain have been noticed and investigated as researchers study the programming of monodomain CAN-LCEs. Similar to disulfide, diselenide bonds are recently developed as one type of novel dynamic covalent bonds. Chen *et al.* applied the rearrangeable polydiselenide networks to fabricate LCE actuators with self-welding properties and sophisticated deformability.[120] Although precious structures and external stimuli are required in the arrangement process, CANs show their fascinating peculiarity and complete the toolbox of achieving monodomain LCEs.

2.2 Molecular alignment of LCEs

Polydomain LCEs are obtained in the absence of external fields and show similar macroscopically isotropic properties as polycrystalline materials. Alignment processes transfer the polydomain LCEs into the monodomain LCEs and premise subsequent phase changes. It was found that chain entropy maximizes in mesoscale N-I transition, thus the regulation of mesophase structures is critical in realizing the high strain response, and ultimately the non-trivial, programmable as well as reversible morphing. The alignment of LCEs into the monodomain or single-crystalline orientation has primarily utilized mechanical stress,[95,105] field-assisted alignments (electric and magnetic field),[121–123] and surface patterning.[30,58] Recently, the new alignment method harnessing 4D printing has been developed; this rheological alignment method will be discussed in Section 3.

Mechanical alignment is the most employed approach to render the orientation of LC directors of gelled networks or the viscous monomer solution. The application of the mechanical field is particularly suitable and effective for 1D or 2D uniaxial alignment of fibers and films. Finkelmann method, first reported in 1991, is a two-stage process that uses stretching and a second crosslinking step to provide a permanent and macroscopically uniform orientation of the domains and thus yields ordered networks.[95] Upon deformation, the partially cross-linked chain segments become aligned according to the symmetry of the uniaxial mechanical stress, then fully polymerized in the loaded state to obtain chain configuration. Yakacki *et al.* extended the two-stage method into a thiol–acrylate Michael addition reaction and subsequent photopolymerization.[105] This stretching-photocrosslink method has been extensively used in generating single-direction deformation of LCEs (Fig. 4a). Despite the homogeneous stretching, anisotropic and inhomogeneous stretch fields can pattern molecular orientations in LCEs during synthesis using multiaxial mechanical forces, hence different active deformation modes are obtained (Fig. 4b).[124]

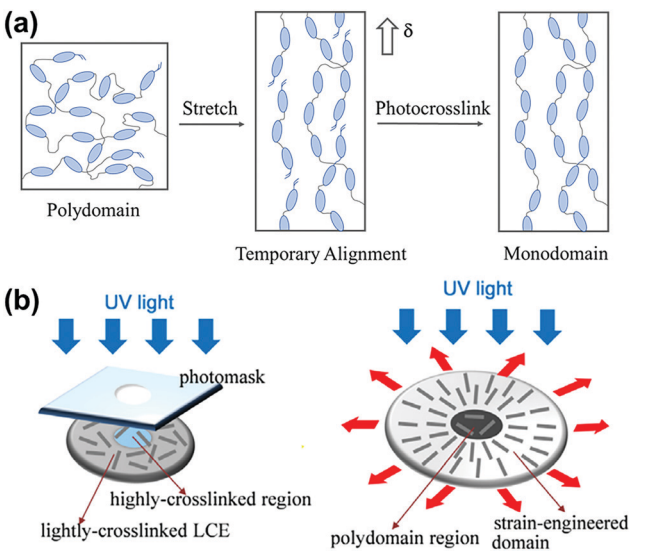

Fig. 4 Mechanical stress-induced alignment. (a) A commonly used two-step alignment of LCE mixtures, which can be temporarily aligned through uniaxial mechanical stretching, and photocrosslink into programmed monodomain. (b) Photomask-assisted inhomogeneous stretching can lead to distinct circular constraints in the LCE sheet. Reproduced with permission.[124] Copyright 2015, Elsevier Ltd.

These methods are proven facile and effective for simple constructs, albeit the mechanical alignment into spatially complex 3D patterns remains a challenge.

Field-assisted alignment is another approach in LCE alignment. LC molecules can orient to electric and magnetic fields owing to their structural anisotropy. The electro-optic response of LCs, especially for the display market, has significantly changed daily life. Unlike low-molar-mass LCs, polymeric LCs require exceptionally high voltages, which may be above breakdown voltages of many composites, for electrical alignment. Thus, electric-field-assisted alignment has been sparingly used in aligning LCEs in planar or homeotropic orientations.[125] Ge and co-workers investigated the thermal conductivity of electric-field aligned LCEs films using ITO glass as electrodes, and the threshold voltage of the tolane–core LCE mixture is 6.82 V μm^{-1}, which confirms the low accessibility of electric control over bulk LCEs.[126] Similar scene occurs in regions of materials subject to magnetic fields, as large fields are required to reach the desired results. Tough aromatics in LC molecules exhibit high magnetic susceptibility perpendicular to the plane of the ring, a magnetic field of 1.2 T for 12 hours is necessary to attest the monodomain conformation of a LCE film with a thickness of 100 μm.[127,128]

Surface patterning relies on the interaction of LC molecules with alignment coatings, also named as command surfaces, to enforce and anchor the orientation of LC molecules by topological entrapment near these surfaces. Unlike mechanical stress and field-assisted alignment, surface patterning can be employed in both high-resolution and scalable production.[129] Generally, surface pattering methods can be categorized into photoalignment, surface rubbing, and lithographic patterning.[30] Photoalignment is an important subclass of surface patterning techniques based on photoresponsive command surfaces that respond to linearly polarized light. One of the main advantages of photoalignment is that photomasks can be harnessed in creating complex director profiles, leading to both in-plane and out-of-plane deformations such as wrinkling, surface depressions, and surface elevations.[130] Common photoalignment materials contain azobenzene dyes, cinnamates, and linearly polarized polymers.[131,132] For example, azobenzene-containing LCE mixtures can determine the molecular conformations with a +1 topological defect and an 8-legged structure, resulting in cone buckling deformation and gripper locomotion upon UV illumination, respectively (Fig. 5a).[58] Another extensively employed alignment method is surface rubbering. Glass slides are rubbed with alignment coatings in one direction to establish the molecular orientation within a plane. Polyimide is one of the most utilized coating materials owing to its anisotropy and the capability of interacting with LC molecules to successfully anchor them.[133] Once the anchoring occurs, the alignment will propagate throughout the LCE solution, leading to aligned domains in LCEs. Ware *et al.* demonstrated topological control over bulk samples by polymerization in surface-aligned slides.[106] A slide was divided into 3 × 3 grids, each including a +1 defect (Fig. 5b). Upon actuation, the flat sheet deformed into "Bowser-shell" geometry that can lift a load of more than 147 times to itself. Additionally, this facile technique can be used to generate a chiral nematic (cholesteric) phase using two slides rubbed with offset directions.[134,135] Previously, glass substrates that sandwich

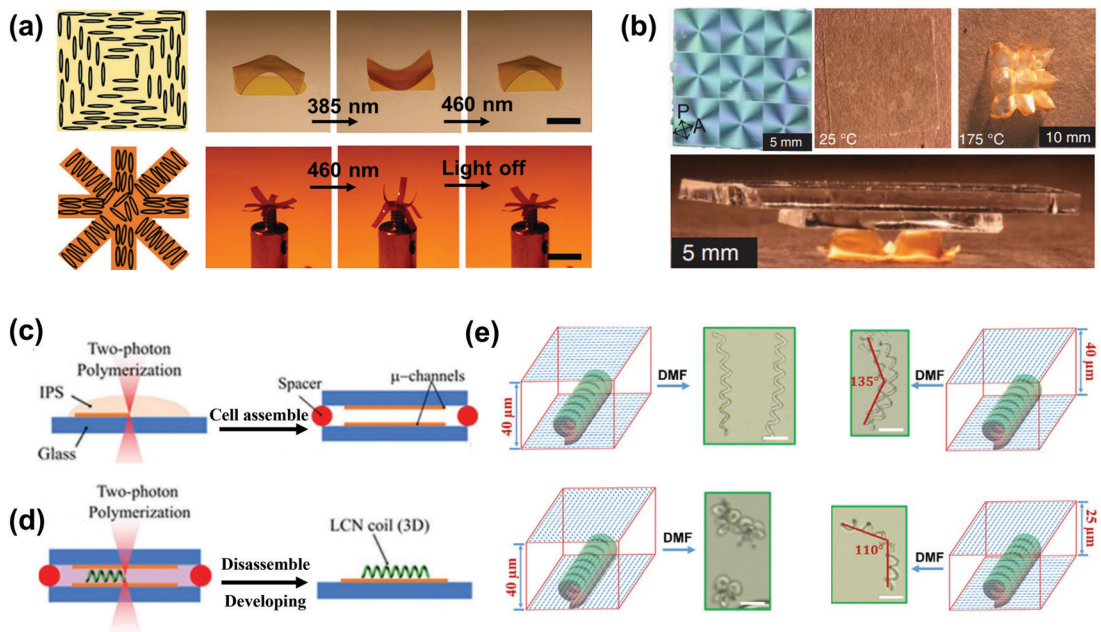

Fig. 5 Surface patterning-enforced alignment. (a) Photoalignment can guide mesogen orientation and achieve out-of-plane deformation (scale bars correspond to 6 mm). Reproduced with permission.[58] Copyright 2017, Wiley-VCH. (b) Surface rubbing is used to generate monodomain LCEs. The sample distorts into cone shapes on glass substrate patterned with +1 defects using polyimide rubbing. Reprinted with permission.[106] Copyright 2015, American Association for the Advancement of Science. (c) Scheme of photolithography of microchannels. (d) Scheme of photolithography of a LCN coil. (e) Various modes of shape transformations from coil-like LCN microstructures. (Scale bar = 50 μm.) Reproduced with permission.[140] Copyright 2020, Wiley-VCH.

the photoresist play a critical role in manipulating the alignment at the surfaces due to the minimization of the Frank-Oseen free energy.[136] Lithography patterns, a hybrid of photoalignment and surface rubbing, have recently been used to attest to the director profile of LC molecules with the rapid development of photolithography.[137,138] Taking the advantages of lithography patterns, micro-structural 3D complexes can be printed layer by layer with the assistance of substrate rubbing, magnetic fields, and surface patterning.[139] Guo *et al.* integrated surface patterning with the SLA technique and exploited the encoding of nematic alignment in topological features with a high resolution of 5 μm by two-photon polymerization (Fig. 5c and d).[140] The orientation control of LCs can be achieved by aligned surfaces through the topography or the chemical structures of a surface that translates anisotropy to the LC fluid. The configurations of director fields and their swelling behavior of coil-like LCE microstructures are investigated, including uniform alignment, twist nematic distortion along the thickness, and sinusoidal alignment on the top substrate (Fig. 5e). The four corresponding shape transformations are differentiated by bending and expansion along helical axes. Higher freedom in the shape programming of LCEs in this strategy greatly expands their applicability in emerging technologies, especially for small-scale soft robots. However, these techniques are typically limited to reasonably thin polymer films (~100 μm) due to the eventual decay of the effective alignments away from the surface.

3. Printing techniques for LCEs

Emerged as versatile material processing platforms, over 50 3D printing technologies have been reported and subclassed into seven categories: binder jetting, material jetting, material extrusion, vat polymerization, powder bed fusion, energy deposition, and sheet lamination.[141] 4D printing technologies are capable of magnifying the characteristics of stimuli-responsive materials and structures. The development of printing technologies is expected to across the constraint that the single-material ink printing hinders myriad conformations and potential applications. To realize a dynamic control of shape heterogeneity in 4D printing, several challenges need to be addressed. First, the proper selection of printing materials requires desirable viscoelastic properties. Second, customers' demands from laboratory to factory necessitate versatile techniques that could print arbitrary shape from microstructures to bulk objects. Third, the initial design of 4D structures also blocks the fidelity and scalability of printed objects. Five main printing technologies have been reported for the 4D printing of LCEs, given the peculiarities of polymeric materials (Fig. 6). Amongst these approaches, DIW is the most extensively studied, owing to its flexibility and rapid printing speed.[142] FDM, another extrusion-based printing technique, has been scarcely reported in the LCE field.[57] Another emerging method is vat photopolymerization, which employs a laser beam or UV light to induce photocuring, including SLA (when a laser beam is used) and DLP (when a projector is used).[59,143,144] Inkjet printing is popular for its cost-effective setup, simple processing steps, and high resolution of 10–50 μm.[145] Multiple print heads can simultaneously spray

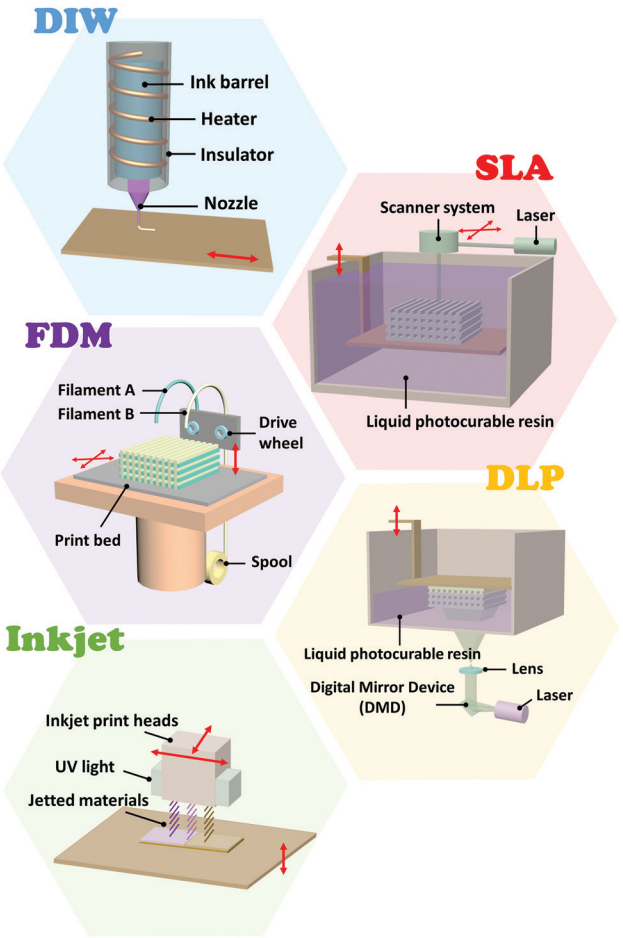

Fig. 6 Schemes illustrating printing techniques for 4D printing of LCEs. Extrusion-based DIW and FDM form 3D projects in a line-by-line and then layer-by-layer manner. Vat photopolymerization-based SLA and DLP can print in sub-micron resolution with high fidelity. SLA employs laser beam and scanner system while DLP relies on digital mirror device (DMD) to achieve dynamic pattern generation. Inkjet printing uses a thermal or piezoelectric actuator to jet materials.

photopolymerizable resins on the printing bed layer by layer and cured by UV irradiation. The impact factors, advantages, and disadvantages of these printing technologies suited for 4D printing of LCEs are summarized in Table 1. These methods have been investigated to adapt to the existent printing technologies and achieve aligned ink during the printing process with the development of 3D printing and increasing demand for LCE printing. Especially, in the past few years, polymers with different cross-linking degree have been printed into sophisticated 3D constructs with localized and voxelated alignment. Herein, we discuss recent research results in elucidating and advancing printing techniques in 4D printing of LCEs.

3.1 Direct ink writing (DIW)

Rheological alignment is another well-known approach to introducing a preferred orientation profile to anisotropic polymer materials.[55] Here, we focus on the exploitation of the rheological orientation of LCs in flow for the 3D printing of LCEs. Concurrent

Table 1 Comparison of common printing techniques for 4D printing of LCEs

	Impact Factors	Advantages	Disadvantages	Ref.
Direct ink printing (DIW)	• Nozzle size • Printing temperature	• Rapid printing speed • Materials flexibility	• Low resolution (50–1000 μm) • The overall structure is composed of extruded arrays, lacking smooth and flat surfaces	56,107,142 and 148
	• Crosslinker concentration • Light exposure time • Light intensity • Beam size	• Cost-effective setups and printing conditions • Printing path dependent • Complex shape changes	• Extra heating system for inks with high viscosity • Photosensitive monomers are required	
Fused deposition modeling (FDM)	• Nozzle size	• Chain ends can chemically crosslink *via* thermal annealing, increasing the molecular weight and stress transfer between filaments	• Low resolution (depends on filaments)	57
	• Annealing temperature • Printing speed	• Outstanding recyclability • Cost-effective setups	• Extra thermal annealing process is required • The core–shell architecture of each filament, fragile along *z*-axis	
Stereolithography (SLA)	• Numerical aperture • Laser intensity • Laser pulse	• High resolution (~100 nm) • Sub-milliseconds response time • Outstanding repeatability • Remotely controllable beam steering • Greater strain-energy dissipation	• Printed structures tend to show slight distortion • Relatively poor fatigue properties • Photosensitive monomers are required • Curing resins need additional care	58
Digital light processing (DLP)	• Light intensity • Light pulse	• High resolution (~10 μm) • High fidelity • Cure a layer of resin at one time and thus can print very fast • High throughput	• Curing resins need additional care • Printed structures tend to show slight distortion • Photosensitive monomers are required	59,143 and 144
Inkjet printing	• Inkjet printing parameters • Light intensity • Light exposure time	• High resolution (10–50 μm) • Single processing steps • Inexpensive hardware and printing conditions • Multi-ink printing	• Slow printing speed • Photosensitive monomers are required	60 and 145

with the new chemistries of LCE synthesis, rheological orientation has been introduced to align bulk samples with relative ease. Additive printing techniques based on the flow of materials include DIW, FDM, and inkjet printing. DIW has proven the best-suited method to prepare the aligned LCEs by printing thus far. Though the chain alignment in 3D objects can be achieved using sophisticated, magnetically and surface pattern-assisted printing or through post-printing programming, DIW is predominantly used in processing LCEs to generate shear-induced orientation nowadays. DIW is based on the ink extrusion from a pressurized syringe to create 3D structures and is commonly employed to print LC monomers while arranging molecular orientation within the extrudate. Functioning as a computer-controlled robot, the syringe head filled with printing ink can move in three dimensions, while the platform remains stationary. 3D geometries are then constructed layer by layer. High operating temperature-direct ink writing (HOT-DIW) is defined by the heat treatment applied while printing to align the mesogenic domains of LCEs. Compared with traditional DIW setups, HOT-DIW uses an additional heater and a thermocouple in the proximity of the printing nozzle to test and control both internal and external temperatures. Then the precursor ink is printed at an elevated temperature range between T_g and T_{NI}. The broad temperature range enables a wide window of orientation degree of LC molecules for 4D printing, which could be characterized by WAXS.[103] The appropriate printing temperature can thus be determined.

To print LCs by DIW, a viscous resin needs to be developed. The limited advances in LCs printing at the primary stage can be attributed to the difficulty in applying proper ink with precise viscosity in the nematic phase. As huge efforts have been paid to this area, the Michael addition reaction between commercially available diacrylates (RM82 and RM257) and primary amine (*n*-butylamine)[49,69,103] or dithiol (ethylene dioxydiethane thiol, EDDET)[117,146,147] has been employed to manipulate the viscosity of LCE resin. EDDET allows for DIW at room temperature, while *n*-butylamine requires HOT-DIW to generate elevated temperatures for desired viscosity. Monomers are partially cured into oligomers, then loaded into the dispenser and heated up to an appropriate viscosity. The shear forces of the syringe that act on the precursor during the printing process align the director along the printing path during printing. In order to finely tune the anisotropy degree

of mesogens, nozzle size including inner diameter, length, and throat diameter, should be carefully selected based on the properties of oligomers. Polymerization is performed by mixing the photoinitiator and other components using mixing nozzles. UV irradiation can be applied throughout the printing process or turned on and off immediately after each layer, thus the mesogenic orientation is locked in.

DIW deposits viscoelastic resins according to a computer-controlled printing path, hence the properties of printed parts will be largely determined by processing parameters including printing speed, temperature as well as photocuring power and time. Ren and co-workers investigated the underlying mechanism of printing speeds and the speed-defined shape morphing behavior.[107] Print speeds at each point could be finely controlled by preprogramming through CAD software. They printed LCE bilayers at average speeds of 3, 6, 9, 12, and 15 mm s^{-1} and characterized the Young's modulus and the order parameter of each sample. Impacted by shearing force, larger printing speeds will generate a greater embedded strain during the shearing flow and stretching force between substrate and syringe tip (Fig. 7a). Fig. 7b demonstrates the possibility of printing a single route with the gradient speeds from 3 mm s^{-1} to 12 mm s^{-1}, which enables the gradually varied mesogenic configuration of LCEs from a larger order parameter to the disordered arrangements. Hence, the local contraction and expansion behavior of different print speeds can be precisely programmed to compose complex shape-morphing patterns (Fig. 7c and d). Resins can be printed under UV irradiation to finish the curing reaction when the photoinitiator is added to activate acrylate end groups.

Temperature is another critical parameter that leads to the variation of viscosity and correlates closely with the quality of printed materials. Wang and co-workers focused on the adjustment of printing temperatures to obtain LCE filaments with tailorable properties, including actuation strain and stress, and mechanical stiffness.[148] Fig. 7e schematically depicts the mechanism of their printing of monolithic fibers. Due to the high viscosity of resins in the cooling process, the reorientation of mesogens is blocked. Thus, for the material near the surface of the filament, the ink temperature rapidly drops to room temperature, fixing mesogens into high alignment before their reorientation. However, for the core part, which is near the center of the filament, the mesogens have enough time to fully rearrange. Consequently, the LCE filament formed a core–shell structure. According to polarized optical microscope (POM) images in Fig. 7f, the volume ratio of core and shell can be finely tuned as demanded when printed at different temperatures. The application of these functionally graded LCE filaments of various actuation strains allows for sophisticated structures to be obtained using the DIW technique (Fig. 7g). Ding and co-workers employed the curing conditions during UV irradiation to control the actuation of LCE.[149] With the built-in compressive strain, the close relationship between printing time and

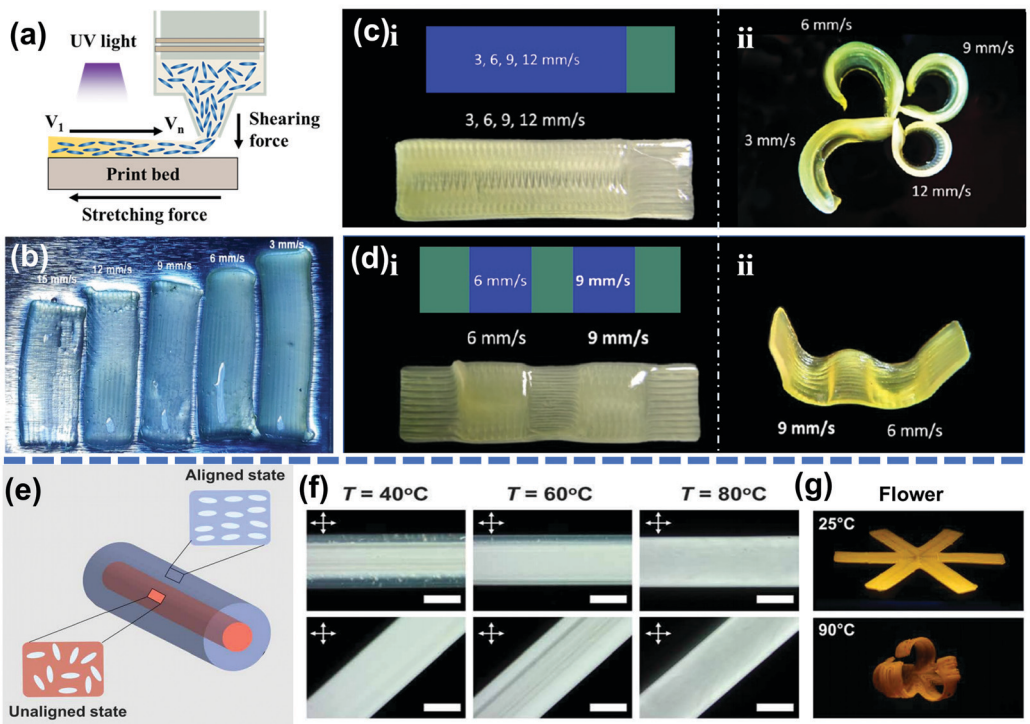

Fig. 7 Parameter-encoded DIW for LCE printing. (a) Schematic illustration of a DIW setup with two types of forces generated during printing, print speeds vary from V_1 to V_n. (b) Distinct shape deformation of strips printed at different speeds. (c and d) Shape-morphing patterns enabled by altering the geometry and print speed distribution of each layer. Reproduced with permission.[107] Copyright 2020, American Chemical Society. (e) Scheme of the core–shell structure of the 4D printed elements. (f) POM images of the printed fibers of different temperatures. (g) Flower pattern composed of two layers with distinct actuation strain. Reproduced with permission.[148] Copyright 2020, American Association for the Advancement of Science.

shape-morphing behavior promises myriad applications of the high-resolution reprogrammable structures.

Compared with other printing technologies, DIW outperforms in materials flexibility, feasibility for multimaterial printing, and high resolution. Solutions, pastes, and gels of different viscosity can all be loaded into ink barrels, thus DIW has been intensely involved in LCs-based printing with different crosslinking degrees. This printing method is also laboratory-friendly, especially when printing nanocomposites with different content of nanofillers or nanoparticles, regardless of whether they are transparent or not.[32,150] Moreover, the required printing conditions and setups of DIW are relatively simple and cost-effective. Despite commercially available DIW printers, labs could build such a platform by themselves with the simple working principle consisting of a computer, dispenser, and substrate. The choices of barrel volume and nozzle size are also flexible according to the demands of researchers.

3.2 Fused deposition modeling (FDM)

Similar to DIW, the introduction of hierarchy can be achieved by FDM, the most common technology for fabricating polymer composites. Both techniques form 3D structures by jointing extruded filaments in a line-by-line and then layer-by-layer manner, while the difference mainly lies in the way they integrate building blocks as a whole. FDM melts solid filaments within the heating nozzle, whereas DIW deposits a viscous ink on the substrate and cures under UV light later. In FDM, filaments are first melted into a semi-liquid state in a syringe and extruded on the stationary platform to be solidified into final objects. The qualities of printed parts can be adjusted by alternating printing parameters, such as the layer thickness, orientation and angles of the printing path, and air gap.[151] One well-known drawback of FDM is that the composite needs to be in a filament state to enable the extrusion, which hinders a uniform reinforcement and void removal. Another disadvantage of FDM printers might be their lack of material selectivity, only thermoplastic polymers with suitable melt viscosities could be finely printed. The molten viscosity should be within the range of providing structural support and enabling extrusion.

However, the disadvantages could also provide opportunities for new-generation anisotropic materials. Gantenbein and co-workers quantitatively explored the mechanism and impact factor of filament-based FDM printing, demonstrating the reinforcement in stiffness, strength, and toughness compared to their state-of-the-art counterparts (Fig. 8).[57] The authors found that filaments generate an anisotropic core–shell structure simultaneously, which partially rearranges the molecular orientation at lower temperatures. Young's modulus of the filaments increases with smaller diameters due to the increasing fraction of oriented polymers within printing lines. Other parameters, such as printing temperatures and solid-state annealing, also contribute to the mechanical properties of LCP fibers. Furthermore, they confirmed that the printed laminates have a comparable stiffness and strength with carbon-fiber-contained polymers, with even better recyclability. The combination of top-down shaping freedom of 3D printing and bottom-up self-assembly of LC molecules shows a broad possibility to fabricate complex geometries of high performance.

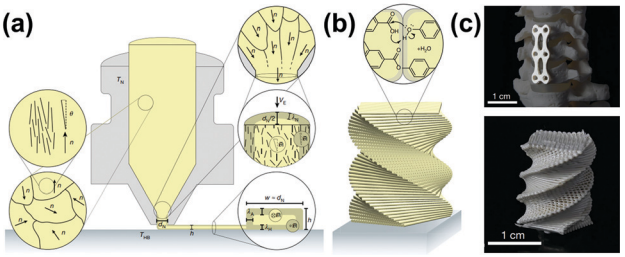

Fig. 8 Hierarchical and thermotropic LCP filaments printed by FDM. (a) The alignment of rigid polymer rods along the director in the melt and the deposition on substrate. (b) After printing, chemical interaction between chain ends *via* thermal annealing leads to higher molecular weight and stress transfer. (c) Photographs of LCP fiber-based complex geometries. Reproduced with permission.[57] Copyright 2018, Springer Nature.

3.3 Stereolithography (SLA)

Photocuring processes, especially radical-mediated chemistries, are widely explored in polymer science, as radicals can transform liquid monomers into solid-state rapidly without organic volatile compounds.[39] Vat polymerization is a photopolymerization-based methodology for 3D printing, which selectively polymerizes liquid photopolymer in a vat, encompassing different subsequent processes such as SLA and DLP.[152] In free-radical photopolymerization, free radicals are primarily generated from two processes: homolytic cleavage is also named as Norrish type I process, while hydrogen abstraction is called Norrish II type process. Typically, homolytic cleavage leads to free radicals that associates with benzyl ketals, including Irgacure 184, Irgacure 651, and Irgacure 369. The unimolecular α-bond cleavage step generates two reactive radicals, allowing for relatively high quantum yields and limited operation windows to UV or blue region. Compared with the type I process, hydrogen abstraction employs bimolecular reactions with electron-donor species, which exhibits a relatively low reaction rate.[153] It is worth noting that LC mesogens contain aromatic rings and double bonds, thus the homolytic cleavage process can be utilized for the formation of free radicals and initiate photopolymerization in the vat.

In contrast to extrusion methods, submicron feature sizes are always possible using vat polymerization techniques. With the increasing demands in integrated functionalities, sophistications, and intelligence, spatial addressing of miniaturized devices in microns and sub-microns is of significant scientific curiosity. Various fabrication techniques, mesogen arrangement methods, and chemical formulations developed in recent years have paved the way for large-scale shape transformation to, albeit the programmable control of local molecular alignments in micro-scale construct remains a challenge.[91] SLA technique has been used for printing LCs of sub-micron feature size, with photoresists composed of LC monomers, a mesogenic crosslinker, and a photoinitiator.[144,154] Zeng *et al.* reported a fabrication method with aforementioned components and additional azobenzene dye to trigger the photo-responsive actuation.[155] Upon irradiation of green light, the azobenzene dye transfers from *trans*

to *cis* configuration, and recovers back from a thermal process.[144] This process is able to actuate a strain of 20% in aligned LCEs within the time scale of milliseconds. Similar to SLA, two-photon polymerization (TPP) also employs a laser beam as the light source for photo-initiated resin curing. However, the special optical process of two-photon absorption demands simultaneous absorption of two photons and thus demonstrating the highest resolution (<200 nm) among all the printing technologies.[156] LCEs are shaped and aligned in the femtosecond process layer by layer, with a limited thickness of around 100 μm.[139] Recently, Guo *et al.* created many cubic light-responsive voxels with predetermined director field orientation by TPP. These voxels can be assembled into various complexes using UV glue, including lines, grids, or skeletal structures.[157] The extremely high resolution of TPP has enabled the sophisticated design of LCE-based microrobots, which can hardly achieve by other fabrication methods.

3.4 Direct light processing (DLP)

Despite laser-based techniques, other photocuring devices have witnessed huge developments. DLP projectors and LCD screens are attractive elements in photopolymerization processes owing to their cost-effectiveness and high resolution. The digital screen is used to simultaneously cure layers of resin with a single image at once with square pixels inside.[158] As a result, DLP can achieve much faster printing speeds, while laser needs to draw out the whole surface progressively. The Yakacki group printed LCE-based dissipative structures with RM 257 and EDDET system by DLP.[59] The printed lattice demonstrates up to 27 times greater strain-energy dissipation than commercial resin upon mechanical testing, leading to large potential in high-energy-absorbing biomedical devices. Using DLP technique, similar systems have been reported with excellent load-bearing performance, which will be further discussed in Section 5.

Analogous to SLA, DLP can be well companied with other alignment methods. Diamagnetic and dielectric anisotropy of mesogenic monomers has been used to arrange a variety of LCEs before crosslinking.[28,123] These techniques are particularly powerful for the uniaxial alignments of microactuators that are too small to be reliably programmed through mechanical methods. Recently, strong magnetic fields have been integrated into DLP technique to obtain voxel-by-voxel encoding of the nematic alignments of LCEs. Shankar and co-workers demonstrated voxelated molecular patterning to direct actuation and manipulation that enable 3D-printed devices utilizing ambient stimuli.[37] This combination of anisotropic magnetic susceptibility in flexible magnetic fields and DLP using DMD presents new opportunities in realizing a local molecular orientation and 3D free-forms, followed by the applications of the light irradiation or elevated temperatures. The programmability over molecule director is realized as magnetic fields reorient alignment, stored by selective freezing *via* crosslinking. A multi-responsive robotic arm can be established by an inverted DLP that polymerizes incremental elements in a bottom-up mode, with multiple printing materials and orientations.

DLP has been previously regarded as a technique to establish polydomain LCP structures that require an align treatment to initiate shape morphing, however, Li *et al.* recently revealed that shear force-induced molecular arrangements can align mesogens during the layer-by-layer DLP printing without any prealignmnet.[143] They attributed this automatic alignment to two reasons. First, the cyclic rotation of the resin tray, which is originally set up to reduce suction force between the build window and printed parts, imposes shear force on the LCE resin while sliding over each thin layer of 20 μm. Second, photocuring under UV light can be asymmetric in height, as part of the actuator (h < 10 μm) is immersed in the resin bath. Monolithic LCE strips show reversible reconfigurations in response to temperature change *via* a built-in shear flow-induced alignment of mesogens (Fig. 9a). High specific work capacity of 63 J kg^{-1} and energy density of 0.18 MJ m^{-3} are realized with a DLP-printed strip. Furthermore, the authors investigated the LCE actuator in a self-sensing system that employs thermally induced optical transition by embedding optical sensing in LCE matrix. In mode 1, the polydomain LCE shifts its color from opaque to transparent under the heat treatment. In mode 2, however, LCE remains opaque in the polydomain state and prevents light beam from transmitting, so that photodetector will not detect signal change. Thereby, a real-time feedback LCE optomechanical sensor is exploited with applicable potentials in the robotics, soft electronics, and medical devices (Fig. 9b).

3.5 Inkjet printing

Despite the familiar usage of printing text and images onto porous surfaces, inkjet printing is known and widely used as a

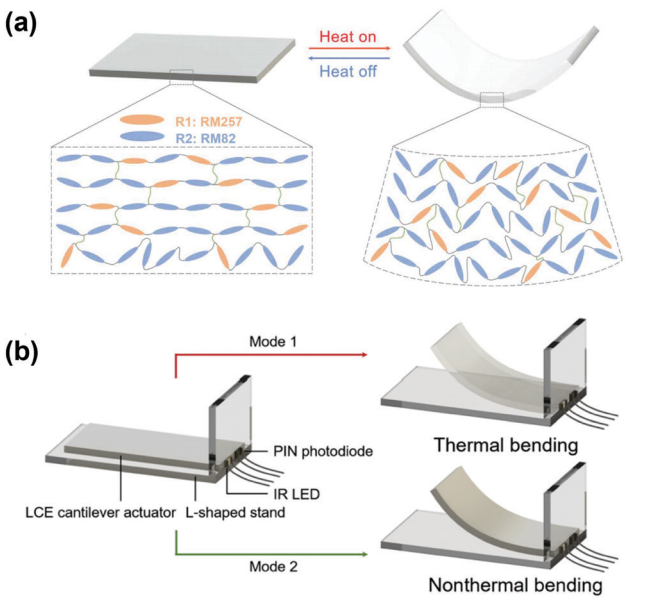

Fig. 9 Thermal bending and optomechanical self-sensing of DLP-printed LCE actuators. (a) Chemical composition and principle of thermo-responsive reversible bending in a layered structure. (b) Schematic of optoelectronic components and LCE cantilever actuator in two modes (thermal bending and nonthermal bending). Reproduced with permission.[143] Copyright 2021, American Association for the Advancement of Science.

freeform fabrication method in 3D printing as well as programming steps for 4D printing.[145] Basically, inkjet printing is a material-conserving deposition process used for fluid.[159] The fixed amount of ink is ejected from the nozzle to the receptor in a chamber. When piezoelectric action occurs, the chamber would contract with external voltage, which leads to liquid drop ejecting from the tip. Inkjet printing has been selected as a process for microstructuring LCE actuators mainly because it allows multi-material ink to be printed in the plane in a single processing step, whereas alternative micropatterning techniques such as vat polymerization may demand more steps to realize the same structures. Oosten *et al.* deposited monomeric LC mixed with two dyes on the substrate using a commercial inkjet printer.[60] In their case, the reactive mixture demonstrated a crystalline–nematic transition above room temperature, and the monomers are therefore printed with optimized molecular alignment to obtain the actuation. The splay-bend configuration enables change of director alignment through the thickness of the film, exhibiting bending behavior by a uniaxially aligned thin film of the same chemical composition by polyimide alignment layer. In addition to simple processing steps, inkjet printing also exploits the self-assembling capacity of LCEs, allowing for scalable fabrication of large-area and roll-to-roll polymer devices and rapid prototyping.

4. Actuation of 4D printed LCEs

LCEs have been regarded as an emerging candidate in stimuli-responsive materials, with intense efforts paid to study the causation between stimuli and actuations. The shape-shifting behavior has become more programmable and promising as 4D printing offers more possibilities for developing complex LCE structures. Intrinsically, LC mesogens would be actuated and change their configuration upon heating, and LCEs undergo large contraction along the nematic director. Actuation methods of 4D printed LCEs mainly include thermal treatment, light irradiation, change of solvent vapor concentration, *etc.* Localized heating can lose space and temporal accuracy due to efficient heat transfer from the source to the ambient environment, instead, light that can generate photothermal conversion and electricity that employs Joule heating has become competitive in initiating thermal responses of LCEs. Other factors, such as humidity change and application of magnetic field, have also been investigated. In this section, we focus on the most recent advances in controllable actuation of different stimuli and the chronological developments in 4D-printed LC-based structures.

4.1 Thermo-responsive LCEs

Heat treatment is the most common stimulus that can simply reduce the order parameter of LCEs. As shape shifting is tied to processing conditions and characteristics of the polymeric networks, the relation between the printing temperatures and T_{NI} leads to reversible processes between the LC phase and the isotropic phase. Thermo-responsive actuation of LCEs has witnessed huge developments in the past five years with various chemistries and recipes. Yuan and co-workers first reported the shape transformation upon heating induced by the silver ink printed on LCE.[53] The laminated structure comprised of printed soft substrates and silver ink, while the LCE strip was pre-synthesized and installed manually. The actuation was stimulated by the conductive Joule heating of the silver ink. When the current was on, the LCE strip was sensitive to the elevated temperatures and showed contraction along the director, inducing the overall bending behavior of the structure. The laminates could also function as hinge materials to activate the two-way deformation of an airplane and miura-ori structures. This work presented the possibility of combining stimuli-responsive polymers with printing systems, though LCE is not directly printed. In 2017, the Ware research group directly printed LCPs *via* DIW for the first time.[49] RM82 and *n*-butylamine are mixed with a molar ratio of 1.1 : 1, which ensured acylate groups at the end of LCE chains. After oligomerization, synthesized ink was printed into various structures and the alignment of molecules agreed with the direction of extrusion. Interestingly, LCE structures are endowed with the out-of-plane and 3D-to-3D′ shape transformations when heated above T_{NI} with spatial programming of the printing paths. Fig. 8a indicates the original design and actuated structures of Archimedean chord and twisted ribbon-like structures, respectively. Kotikian *et al.* used the same monomer and amine chain extender to synthesize LCE ink *via* aza-Michael reaction except at a modified molar ratio of RM 82 : *n*-butylamine at 1 : 1 to tailor the phase transition temperature, and successfully decreased the T_{NI} to 95 °C.[103] Similar chemistry has been employed by Lopez-Valdeolivas and co-workers for the integration of printed LCP and PDMS to fabricate an asymmetric structure to illustrate the possibility of LCs to serve as a focus lens.[69] The contraction of LCEs led to convex on one side and concave on the other side of the structure when heated. The focusing properties could thus be simply tuned, which demonstrated the potential of LCEs as optical components. As mentioned above, when the crosslinking locks the programmed molecular orientations and efficiently stabilizes the nematic configuration, the energy needed for a phase transition is elevated. To build up sophisticated structures with heterogeneity in a wide temperature window, the Ware group concentrated on tuning crosslinking degree and exploited a dithiol–ene reaction for ink fabrication and printed 3D structures with tunable actuation temperature (28 ± 2 to 105 ± 1 °C) *via* different selections of thiol spacer and the weight ratio of the LC monomers (RM82/RM257).[104] Though these processing methods dramatically enlarged the temperature window of actuation and facilitate ink preparation, the shape transformation remained a proof-of-concept with limited real-life significance. Recently, Kotitian and co-workers reported an origami-based strategy for designing soft robots that exhibit shape changes through a reduced set of predictable motions.[67] Localizing deformations to creases, actuating hinges that connect with planar facets were used to simplify the design space. Two kinds of hinges (LT_{NI} hinge and HT_{NI} hinge) that display different actuation temperatures introduced an additional degree of freedom for

the robots, in which the LT_{NI} LCE hinges induced folding into a pentagonal prism and the HT_{NI} hinges propelled the robot when heated above their actuation temperature (Fig. 10a). A sequence of still images shown in Fig. 10b confirms the gradient-driven propulsion to continue the motion even after the shape deformation to a full roll. The printed structure travelled 12 cm in 95 s without a need for manual reprogramming. The simple but effective method can be expanded to the passive control of soft robotics and, ultimately, robots with more complex functionalities and locomotive tracks. Zhai and co-workers developed an untethered soft robot capable of complicated locomotion when heated to above 160 °C, such as transforming, rolling, and climbing.[160] The active bilayers are perpendicular to each other, with an overall printing direction at an angle of 45° to the long axis (Fig. 10c). Particularly, heating causes incompatible strains in the LCE film, leading to an out-of-plane morphing into a tubule. Owing to the existence of the temperature gradient, the bottom and top of the circle shrinks and extends, respectively, disturbing the balance of forces and rendering the sample with the rolling ability. A 10 cm-long robot can attain a maximum velocity of more than 48 cm min^{-1} both on the horizontal plane and climbing a slope of approximately 20°.

Despite variations in the chemical composition of LC oligomers, additional networks have been introduced to the LCE matrix to regulate the arrangements of mesogens effectively. CANs have been introduced in fabricating LCEs in the most recent decade, which undergo exchange reactions with or without exerting stimuli. The repeatable, reversible, and recyclable bond exchange allows for stress relaxation, surface self-healing, and a high degree of tailorability.[102] In addition to programmability, dynamic covalent bonds endow LCEs with great recyclability, self-healing abilities, and reprogrammability.[161] Davidson *et al.* employed radical-mediated dynamic bond exchange into the LCE network in order to create a printable and reconfigurable ink.[117] The prepared ink consists of RM82 and a mixture of allyl thiol and EDDET. Allyl thiol undergoes efficient bond exchange in the presence of radicals, while EDDET functions to suppress the crystallization and decrease the T_{NI}. The dynamic structures are transparent due to the alignment of LC domains. Thermal actuation happens in a wide temperature range and the contractile strain along the director achieved 50%. The actuated shape would maintain at the ambient temperature when programmed LCE structures with dynamic bond exchange were actuated under UV irradiation. Further thermal cycling only initiated the optical

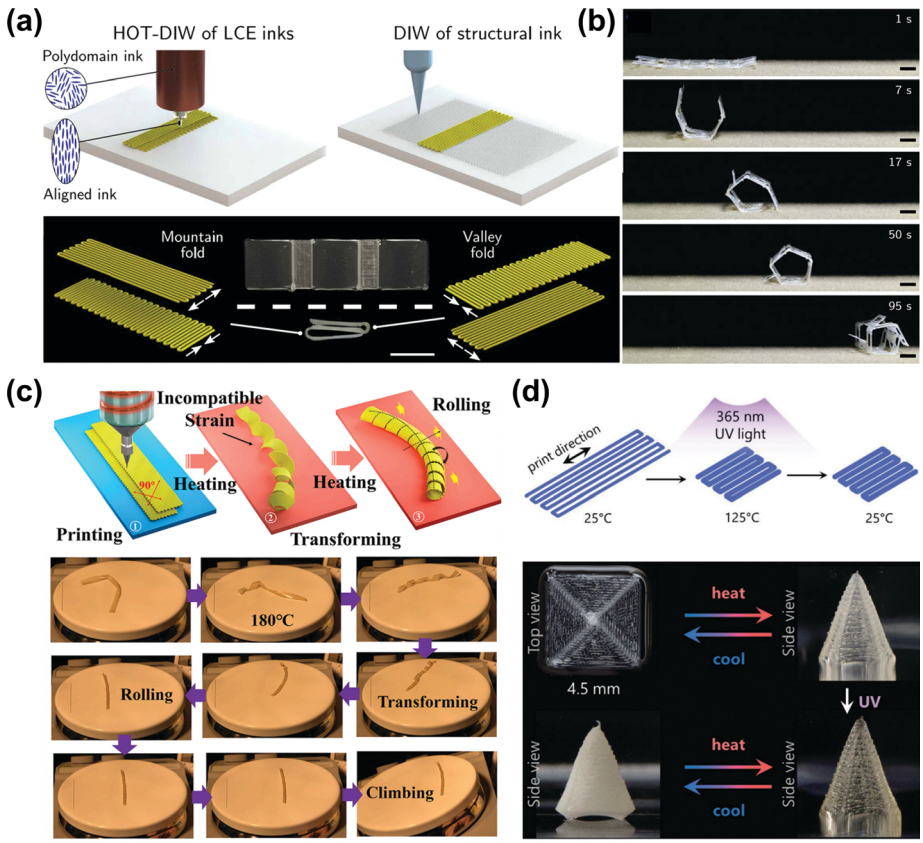

Fig. 10 Thermo-responsive actuations of 4D-printed LCEs. (a) Schemes of the printing of LCE inks and structural inks, respectively. Mountain fold and valley fold can be achieved by different printing paths. (b) Image sequences of the self-propelling locomotion of the robot (scale bar = 1 cm). Reproduced with permission.[67] Copyright 2019, American Association for the Advancement of Science. (c) Mechanism and self-propelling behaviors of 4D-printed untethered bilayer LCE soft robots, including transforming, rolling, and climbing. Reproduced with permission.[160] 2021 Elsevier Inc. (d) Schematic view and images of LCE samples after printing, heat treatment above T_{NI}, and UV-assisted locked-in reconfiguration. Reproduced with permission.[117] Copyright 2020, Wiley-VCH.

change between transparent and opaque states, which was attributed to the break of inner alignment, with shape deformation remaining (Fig. 10d).

4.2 Photo-responsive LCEs

Since the semiconductor industry pioneered topologically patterned surfaces in 1970s, photonic technologies have developed rapidly in the following decades. The relationship between light and matter is considered of vital importance in the reliable production of patterns with high resolution. Serving as remote control over space and time, light irradiation can initiate chemical reactions that would otherwise not occur in ambient conditions. Thus, light is gradually harnessed as an effective tool to structure polymeric materials and open new horizons for technological progress in different fields. Typically, UV irradiation initiates the polymerization by generating free radicals that are associated with benzyl ketals in the presence of photoinitiators. Despite this necessary setup of photopolymerization, light could serve as the remote control of LCE-based actuators. Light outperforms heat in several aspects including the high resolution, the fast speed at small scales, and tunable properties such as wavelength, intensity, exposure time, and polarization.[162,163] In the following, we present the recent examples that are actuated by light.

Two predominant mechanisms have been involved in photo-responsive actuations. First, the photothermal effect can be utilized to initiate the actuation of LCEs as a substitution for traditional heat treatment. With the assembly of carbon nanotubes (CNTs),[164] graphite oxide (GO),[165] MXene,[166] gold nanoparticles (AuNPs),[167,168] and dyes,[68,169–172] the order parameter of LC mesogens are reduced by the heat generated in the photothermal conversion process. However, these nanomaterials show poor compatibility with LCEs with their inorganic nature. Second, isomerization proposes a reduction of molecule length from *trans* to *cis* states. This process is typically induced by UV light or visible light near the UV region. For example, UV exposure leads to fast *trans–cis* transformation of azobenzene derivatives. Specifically, azobenzene derivates show strong absorbance within UV ranges and weak absorbance within visible ranges at the *trans* state, while *trans–cis* isomerization leads to stronger absorption in visible light. Visible light hence undergoes manipulation of backward *cis–trans* isomerization due to the higher absorbance. When LCs are modified with azobenzene moieties, they can be stimulated by UV light. The *trans–cis* transformation disturbs the alignment of LC mesogens and reduces the order parameter as the lengths of molecules are shortened to 5–6 Å from the original lengths of 10–20 Å.[169,170] As a result of slow photon accumulation, this method shows a relatively slow actuation speed compared with photothermal effect.[171] Additionally, the relaxation of the *cis*-isomer of azobenzene over time results in short-lived deformation in azobenzene-functionalized LCEs, which impedes their utility and requires constant energy expenditure for shape maintenance. Lu *et al.* 4D-printed shape-switching LCEs functionalized with dynamic covalent crosslinks and azobenzene to tackle this problem.[68] Specifically, ureido-pyrimidinone (UPy) self-associates into dimers with a relatively high bonding energy of 50 kJ mol^{-1}.[172] UPy dimers favor the dissociation upon the photothermal effect, hence crosslinks would lock the shape change (Fig. 11a). Diels–Alder crosslinks enable photoactuation at a temperature much lower than the printing temperature and the amount of the DA bonds and UPy could be used to tune the T_g and T_{NI} based on requirements. The photothermal effect heats the illuminated region above the UPy dissociation temperature upon UV irradiation. On removal of the light, the *cis*-isomer persists for hours, but the UPy crosslinks reform immediately as the sample passively cools. Hence, the photothermal effect enables the adaptive reorganization of the polymer networks to lock the shape change, as shown in Fig. 11b. This technology fixes shape-switching LCEs with more than 90% of deformation over 3 days, impacting new prospects such as deployable devices where the continuous application of power is impractical.

Micrometer scale robots, which demand a high printing resolution, flexibility, and wireless control, have been proposed for various applications including drug delivery,[173] biosensing,[174] and microsurgery.[175] Zeng and co-workers presented a microscopic walker that can overcome the van der Waals force between its legs and the surface it walked on.[176] The walker consisted of a homogeneously aligned LCE body with slightly tilted legs attached to it, while the legs were printed with a rigid, commercially available acrylate resist called IP-Dip. The LCE body contracted, and the legs moved towards each other in the line of the director when the green light was shed onto the walker. Recently, Chen and co-workers reported near-infrared (NIR) light-powered 4D microstructures with enhanced mechanical properties using DLP technology, as illustrated in Fig. 11c and d.[139] The nematic-to-isotropic transition of the LCE nanocomposites happens when exposed to NIR irradiation based on the photothermal effects of gold nanorods (AuNRs) and the miscibility between AuNRs and LCE is enhanced by thiol functionalization. Fig. 11e shows the shape deformation and restoration process of AuNRs/LCE. A 3 wt% loading of additional particles could lead to as much as 20% elongation under a NIR laser power of 2 W.

4.3 Electro-responsive LCEs

The employment of electricity has been a symbol of human development as well as scientific advances. The utilization of electricity in powering soft actuators has been extensively explored as controllable green energy. Electrothermal feedbacks that arise from Joule heating can be an optimal strategy due to their controllable and sensitive responses to embedded stimuli. Through the integration of conductive fillers such as carbon black particles and CNTs, LCE composites show electrothermal heating, which generates the heat needed to disorder aligned mesogens thus actuating shape switching.[177–179] However, high loadings of the fillers are required in these approaches to form percolated networks through the elastomer matrix, which may hamper the shape changes and multi-path printing, especially for 4D printing. LCE composites with dispersed CNTs, for example, can be aligned during extrusion at compositions up to 2 wt% to create photothermally active composites, but this amount is insufficient to induce electrical conductivity.[179]

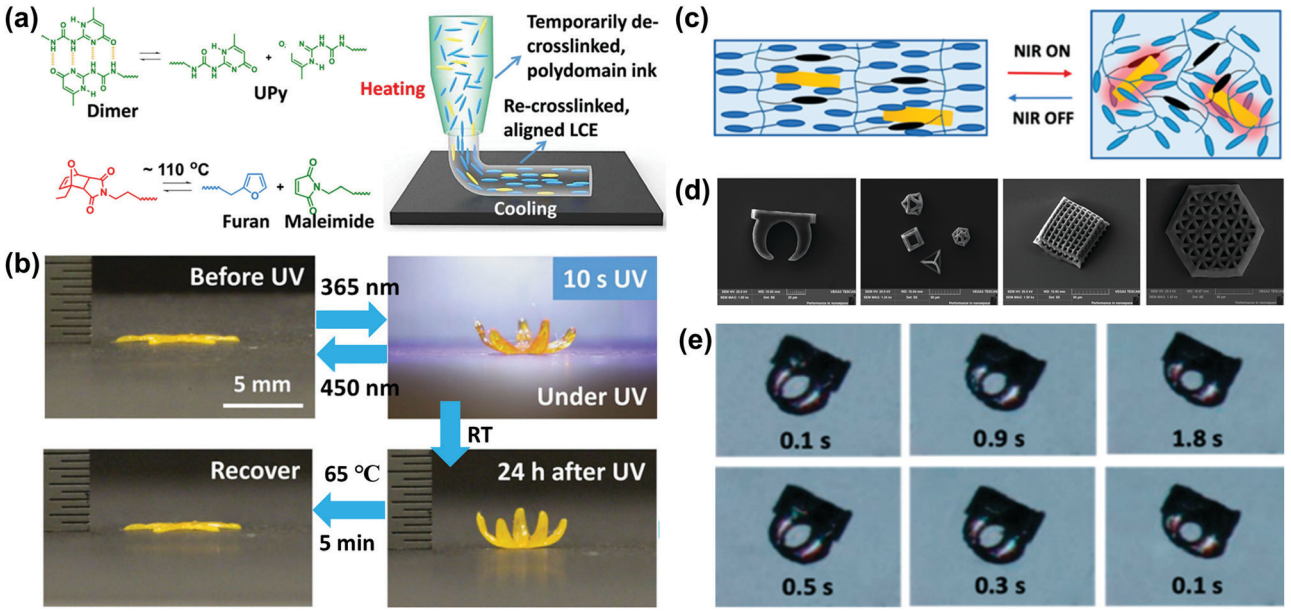

Fig. 11 Photo-responsive actuations of 4D-printed LCEs. (a) Chemical composition and illustration of LCE ink printing with dynamic feature. (b) Photographs of photoswitchable shape deformation of flower-like actuator. Reproduced with permission.[68] Copyright 2021, Wiley-VCH. (c) Mechanism of the reversible NIR-responsive shape deformation behavior of the AuNRs/LCE. (d) SEM images of the 3 wt% AuNRs/LCE 3D microstructures fabricated using DLW. (e) Shape deformation and restoration under phase transition. Reproduced with permission.[139] Copyright 2019, American Chemical Society.

Carbon black-filled LCEs can also be electrothermally heated when the high concentration of fillers are included (15 wt%), while these materials exhibit decreased actuation strain from 35 to 5.2%.[180] Fundamentally, the use of electrically conductive fillers could not balance the trade-off well between electrical conductivity and valid shape change.

Recently, the integration of resistive liquid metals (LMs) with LCEs for Joule heating has witnessed an exponential growth. High electrical conductivity, thermal conductivity, excellent biocompatibility and fluidity have rendered LMs with great potential as functional materials.[181,182] Eutectic gallium indium (EGaIn) is a commercially available alloy that exists in a liquid state at room temperature while featuring metallic high electric/thermal conductivity. Typically, the resistivity of bulk EGaIn is around $\sim 29.4 \times 10^{-6}$ Ω cm, and the viscosity at room temperature of $\sim 1.99 \times 10^{-3}$ Pa s. These fascinating properties make this material particularly promising for resistive heaters, stretchable circuits, and flexible sensors.[183] Lv and co-workers unprecedentedly reported a nanocellulose-based colloidal LM ink for shape-deformable and electrically conductive LCE soft robots that can be electro- and photo-thermally actuated.[184] However, an effective and facile approach to combining LM and LCE in 4D printing remain unsolved in the past years. Ambulo *et al.* developed a 3D-printable LCE matrix dispersed with liquid-metal (LM) droplets to preserve the compliance and shape-morphing properties of LCEs.[150] This process enables dual-actuation of photothermal and electrothermal response. LM-LCE networks with a lower LM concentration (71 wt%) exhibited a photothermal response to NIR light irradiation, while a higher concentration (88 wt%) allowed for electrical Joule heating of LCEs. Another intriguing work done by the Lewis research group at Harvard University provided an avenue for efficiently coupling LCE systems with resistive LM to enable Joule heating.[185] DIW method extrudes coaxial filaments with LM core surrounded by a LCE shell, whose director is well aligned along the print path (Fig. 12a and b). As the inner LM forms a closed circuit with copper wire, the resistance of LM and the overall length of the innervated LCE actuators (iLCE) change with respect to shape and temperature. The thermal response of the fiber-type actuators is measured with discrete power inputs from 1 to 40 mW mm^{-2} (Fig. 12c). Impressively, when an input power of 40 mW mm^{-2} is applied, the iLCE can be rapidly actuated, with over 90% of their maximum contractile strain achieved within 10 s. A closed-loop control system is programmed with a target configuration overtime to characterize this reversible resistive feedback when cycled between off and on (5 mW mm^{-2} and 15 mW mm^{-2}) power input (Fig. 12d). It is demonstrated that the iLCE is capable of tracking self-regulating actuation while escaping from large disturbances of 4.2 g, which is over 115 times the bodyweight of itself.

4.4 Other stimuli-responsive LCEs

Beyond the direct heat treatment or light- and electricity-induced conversion, other stimuli could also actuate large-scale and designable motion of LCEs, which enlarges the toolbox of the LC-based sensors and soft robotics.[186] Water- or humidity-responsive properties have been integrated into LCEs using several strategies. A single-layer humidity-responsive LCN with carboxylic acid groups was first reported by the Broer group in 2005.[187] A subsequent alkaline treatment disrupted the hydrogen bonds in the LCN and generated carboxylate sodium salts, making the LCN hygroscopic and humidity-sensitive. The local treatment of the LCN by an alkaline solution enabled the design of shape-programmable humidity-responsive actuators that can

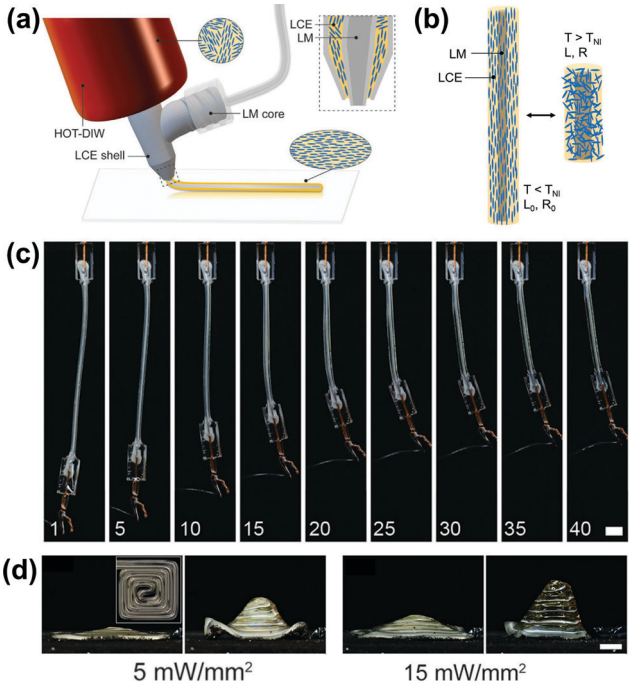

Fig. 12 Liquid metal-enabled electro-responsive 4D-printed LCE actuators. (a) Scheme of core–shell iLCE fibers composed of LM core and LCE shell. (b) Scheme of iLCE actuation when cycled above and below T_{NI}. (c) Optical images of electrothermally actuated iLCE fibers with discrete power inputs of 1 and 40 mW mm^{-2} (scale bars = 5 mm). (d) 3D actuation of iLCE spiral structure with closed loop control. Reproduced with permission.[185] Copyright 2021, Wiley-VCH.

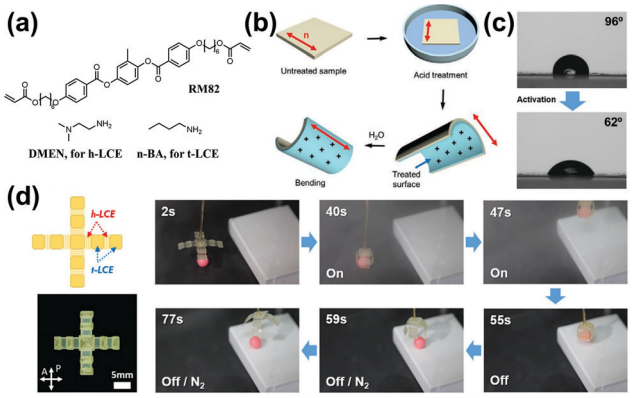

Fig. 13 Humidity-responsive 4D-printed LCEs. (a) Chemical composition of h-LCE and t-LCE. (b) Schematic of monodomain h-LCE activation by acidic solution (0.1 M HCl) and its bending behavior upon exposure to moisture. (c) Contact angles of h-LCEs before and after acid activation. (d) LCE soft gripper integrating both h-LCE and t-LCE. Grabbing, transporting, holding, and releasing functions are achieved by humidity control. Reproduced with permission.[193] Copyright 2021, Wiley-VCH.

bend, fold, and curl. Bilayer approaches include two films showing different behavior in response to a specific humidity environment. Schenning and co-workers spray-coated chiral nematic LCs to polyamide 6 (PA6) substrate, followed by photopolymerization.[188,189] The preprogrammed handedness and the extent of helical twisting allow for a complex shape morphing in response to humidity change. The Ware group took advantage of hydrophilic poly(ethylene glycol)diacrylate (PEGDA) to couple water absorption of hydrogels with the inner anisotropy and thermal actuation of LCEs.[186] In a similar vein, Yang and co-workers integrated hydrochromic aggregation-induced emission molecule-doped poly(acrylic-*co*-hydroxyethyl acrylate) (PA) layer into LCN systems.[52] Under the different relative humidity, the composite films can deform and change fluorescence color simultaneously. Apart from that, dual-responsive LCE actuators that are sensitive to moisture as well as additional external stimuli, including temperature,[189] light,[190,191] and gas have been reported to provide multifunctions.[192] Kim *et al.* raised a class of novel hygroscopic LCE actuators that achieves self-alignment by various fabrication methods from surface alignment to 3D printing, dramatically expanding the geometry complexities and possibility of scalable production.[193] Using the same LC monomer, RM 82, the authors utilized *N*,*N*-dimethylethylenediamine (DMEN) and *n*-butyl amine for the preparation of humidity-responsive LCE actuators (h-LCEs) and thermo-responsive LCE actuators (t-LCEs), respectively. Opposite to previously mentioned actuators containing carboxylic acid groups, acidic solution was employed in this work to generate cations on the surfaces and provide asymmetric hydrophilicity to the LCEs (Fig. 13b and c). The protonation of dimethylamino groups happened with the activation step in aqueous HCl, so the asymmetric moisture sensitivity and moisture adsorption formed on the activated surface of h-LCE. DIW enabled both surface alignment and shear alignment in hygroscopic LC systems and created several sophisticated architectures with a wide range of applications in soft robotics. Fig. 13d exhibits a sequence of motion achieved by the LCE soft gripper composed of h-LCE and t-LCE, showing rapid and precise response upon the control of atmospheric moisture.

Magnetic field as a kind of important physical field has gathered increasing attention for scientific research, with the rapid development of electromagnetic technology and permanent magnetic materials. The noncontact, highly controllable, nondestructive control allows for flexibility and reversibility during the applied process.[194] Therefore, the research concentrating on magnetic-field-induced effect have emerged and demonstrated intriguing functionalities within LCEs. Sitti and co-workers have reported a monolithic composite film that integrated magnetic microparticles inside the LCE matrix.[123] The remote magnetic field enables untethered *in situ* soft miniature machines, without breaking the formation of helices. Another inspiring work done by the Sitti group is dual-responsive biomorph materials. They incorporated a magnetic-responsive elastomer layer and a LCE layer, which offers abundant degree-of-freedoms due to the programmable director field of LCEs, controllable magnetization profile of magnetic-responsive elastomer, and diverse geometric configurations.[195]

5. Emerging applications of LCEs

Despite the rapid development of printed LCE-based smart actuators, other emerging applications, such as biomedical

devices and optics, have been brought into focus in recent years. The tailorable properties and dynamic control of LCEs have enabled the anticipated technologies in these nascent fields. We herein introduce the latest development of 4D-printed LCE constructs for their emerging applications other than actuators and robotics, with emphasis on optical devices and the biomedical world, to motivate inspiring thoughts and deployable devices involving LCEs.

5.1 Optical applications

Over the years, chameleon-mimicking full-color camouflage has maintained scientific interests due to its potential in anti-counterfeiting, smart coatings, and military use.[196] Anisotropy in LC mesogens provides heterogeneous properties along the horizontal and vertical directions of LCEs. Cholesteric liquid crystals (CLCs) are considered one-dimensional photonic materials with a unique light manipulation.[197–199] The helical molecular organization of CLC polymers exhibits selective reflection of left- or right-handed circularly polarized light at a wavelength comparable with visible light, thus enabling macroscopic color change.[200] Inkjet printing has been used to assist the establishment of CLC polymers for complicated and diverse patterns. Moirangthem *et al.* prepared a blue reflective CLC polymer coating and reported a full-color pattern method for the first time.[201] The printable coating was synthesized from a monomer mixture consisting of diacrylate and monoacrylate mesogens, among which hydrogen-bonded benzoic acid-functionalized 6OBA and 6OBAM were used as ligands to bind calcium ions. By printing $Ca(NO_3)_2$ solution as the ink, the polymer coating can be patterned from blue to red, over the entire visible spectrum. The elimination of nonreactive low-molar-mass 5CB leads to shrinkage in the helical pitch of CLC polymer. Patterns with various amount of Ca^{2+} ions swell differently in the wet state, hence the color is hidden behind the blue color in the dry state and appear in the wet state. A flower pattern has been printed by varying the helical thickness, with a Ca^{2+} solution at the same drop spacing of 20 μm (1270 dpi). The pattern stayed hidden in the dry state and occurred upon water exposure with high resolution. Similarly, Yang and co-workers exploited a printable polymer fabricated from a liquid crystalline blue phase network.[202] Arbitrary colors could be patterned and erased reversibly, making this coating promising as rewritable papers and low-molar-mass LC responsive materials.[203]

Unlike the above-mentioned full-color camouflage generated by inkjet printing, Sol *et al.* prepared an ink with free-forms in iridescence and circular polarization selectivity of reflected light.[204] Characteristic demonstrations of the polymer films are based on the incidence angle (Fig. 14a). While the optical response of conventional right-handed CLC film reflects 100% right-circular polarized light and no left-circular polarized, the bar-coated film reflects only 35–40% of both at λ_{max}. A slanted configuration, rather than a cholesteric helix, is proposed schematically in Fig. 14b. With the distortion in photonic periodicity, the CLC ink was applied to print chiroptical patterns. On the side of processing, DIW allows for alternative deposition rates

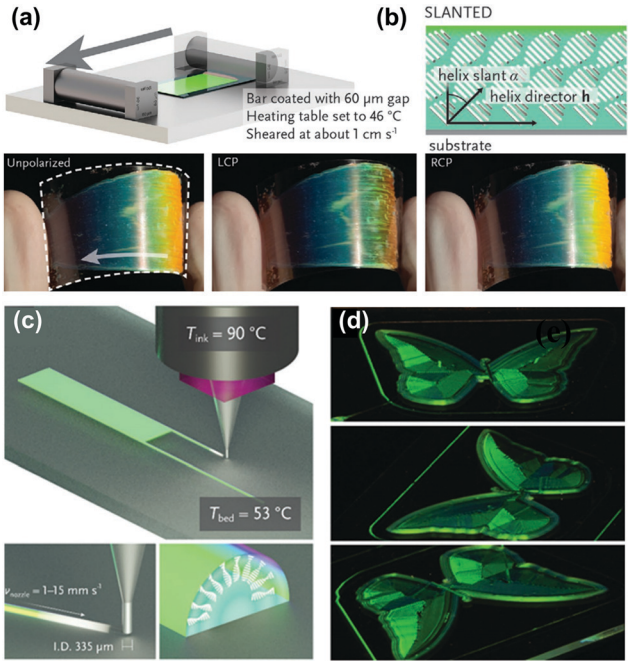

Fig. 14 Anisotropic iridescence and polarization in DIW-processed CLC photonic polymers. (a) Bar-coating process and axially asymmetric color reflection and circular polarization selectivity of crosslinked CLC photonic films. (b) Scheme of the molecular alignment in a slanted helix director. (c) Scheme of DIW process and the molecular structure for the cross-section of an ideally aligned fibril. (d) Butterfly structure observed from various directions. Reproduced with permission.[204] Copyright 2021, Wiley-VCH.

and hence anomalous optical properties of the printed parts, leading to spectacular visual effects from a single ink material (Fig. 14c). A planar alignment is prone to form at low lateral nozzle speeds, while a slanted configuration occurs as the speed increases. A Morpho-inspired butterfly structure is printed using multiple printing speeds, with 2 mm s^{-1} for the rim and 10 mm s^{-1} for the inner area. A visible transition from planar to slanted helicoidal alignment endows the butterfly with special visual appeals (Fig. 14d). The employment of DIW technique for the generation of intricate optical patterns offers the possibility of anomalous chiroptical properties of the ink, paving the way for the design of polymeric elements with disparate optical effects using the same ink within a single print.

5.2 Biomedical applications

Stimuli-responsive materials have long been designed to meet the requirements of biomedical devices as their salient dynamic features can augment or replace the behavior of natural tissues.[205,206] So far, no medical device composed of LCEs has been approved for human use by the US Food and Drug Administration.[207] However, prospective investigations have been proposed in the past few years for their biomedical applications, including microscale actuators as surgical tools, orthopedic implants, and cell culture.[41] Here, we summarize the ways that LCEs have been prospective for biomedical applications, thereby motivating the advancement of novel roles for LCEs.

5.2.1 Energy-dissipative materials. Most load-bearing biological tissues (*i.e.*, bones, muscles, and connective tissue) demonstrate anisotropic and heterogeneous mechanical properties with their complex hierarchical structures. LCEs can be fabricated with both the polydomain and monodomain regions of various inner molecular orientations. The resulting materials would show elastic behavior in certain areas while exhibiting energy-dissipative properties in other regions, which can mimic the properties as well as physiological functions of organisms. Typically, LCE-based structures can exhibit remarkable mechanical properties, which display load-bearing and energy-absorbing characteristics. Yakacki and co-workers have 3D-printed a semi-crystalline LCE fusion cage for the treatment of degenerative disc disease.[71] While most traditional spinal fusion techniques fail for insufficient immobilization of the vertebrae, this methodology addresses subsidence challenges *via* a dynamic behavior during and after implantation. The deformable, rubbery LCE which well conforms to anatomy, crystallized into a rigid, structural material in the following several hours, with Young's modulus increasing from 8 to 80 MPa. The crystalline regime presented reversible compressive loading of more than 1 million cycles, informing a proof-of-concept bulk 3D LCE device. As such, another work done by this group introduces an inter-vertebral disk model LCE, consisting of the polydomain region that mimics the mechanical damping of the nucleus pulposus central part.[208] The selective reorientation of the polydomain provides energy absorption and soft elasticity to the disk replacement when loaded with weight.

Despite these implant materials, LCE-based energy-dissipative structures have attained special attention due to the geometric tailorability of the 3D-printed lattices and precise control over mechanical and dissipative properties. Yakacki research group has reported DLP-printed high-resolution energy-dissipative lattices with micro- and macroscopic architectures.[59] Compared with commercially available photo-curable elastomer resin, the stress-strain responses of LCE lattices have exhibited 12 times larger rate-dependence and 27 times greater energy absorption. Further, this group has used DIW to fabricate bulk monodomain LCEs and investigated their compressive soft-elasticity over 8 decades of strain rate.[209] The rotation of the anisotropic polymer conformation gives rise to the tensile soft-elastic response of LCEs, which bears resemblance to the idealized load curve of a strain-energy absorbing device (Fig. 15a and b). At quasi-static rates, the monodomain soft-elastic LCE dissipated 45% of strain energy while comparator materials dissipated less than 20%. At strain rates up to 3000 s^{-1}, the sample consistently performed closest to an ideal-impact absorber. Similarly, Yu and co-workers used DLP to control the mesostructures within the LCE foam with polydomain. The mechanically induced phase transition under large strains added a second energy dissipation mechanism to

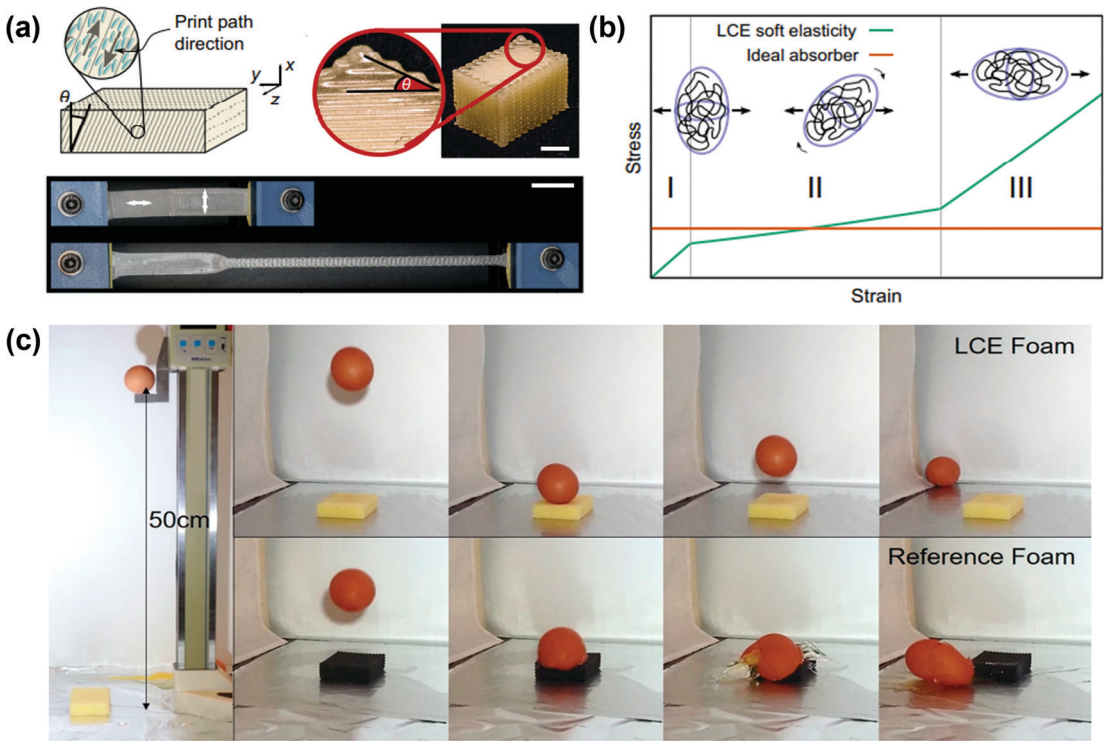

Fig. 15 4D-printed energy-dissipative materials. (a) An example of a bulk 3D-printed LCE, optimization of the print conditions allows high-quality printing of bulk devices. The direction of print head movement dictates the orientation of the liquid crystal director. (Scale bar = 5 mm.) (b) The rotation of the anisotropic polymer conformation gives rise to the tensile soft-elastic response of LCEs, which bears resemblance to the idealized load curve of a strain-energy absorbing device. Reproduced with permission.[209] Copyright 2021, Springer Nature. (c) Images series of egg dropping onto a LCE foam from a 50 cm height. The elastomeric foam protected the egg from breaking. Reproduced with permission.[210] Copyright 2020, American Chemical Society.

the solid matrix, in addition to the viscoelastic relaxation of the polymer network.[210] Higher axial strains are achieved when increasing the lattice connectivity, on account of a larger mesogenic reorientation in stretching-dominated deformation than in bending dominated process. The foam is capable of protecting an egg from breaking for a drop height of 50 cm (Fig. 15c). The outstanding energy absorption during the repeated dynamic loading has significantly extended the potential of LCEs to protect physical protection systems against mechanical impact. Jeon *et al.* recently reported that the energy absorption density of architected LCE materials increases with strain rate according to power-law relationship.[211] With this newly obtained knowledge, they achieved a 5 MJ m^{-3} energy absorption density at a strain rate of 600 s^{-1}, which is two orders of magnitude higher than previously reported results.

5.2.2 Cell culture. Control over cellular alignment and organization is of vital importance in tissue engineering. With the innate molecular organization, LCE coatings have been used as tissue scaffolds to induce cellular alignment. Agrawal *et al.* introduced LCE nanocomposites (LCE-NCs) with a fast and reversible electrochemical response, which can be leveraged as dynamic substrates for the cell culture.[180] When used as a responsive substrate to culture neonatal rat ventricular myocytes, the cells remain viable on both stimulated and static LCE-NC substrates. This opens a new avenue in engineering substrates for cell growth with not only predetermined alignment but also control over their cellular organization. In addition to orienting cells through topographic cues, the reversible shape changes of LCEs can be employed to induce dynamic cell alignment. As many biological tissues are subject to reconfigurable mechanical deformation during the development and normal function, a reprogrammable environment that provides stresses and strains similar to those in the body to cells would succeed in maintaining cell activity and phenotype. In properly designed culture environments, the heat capacity of water can neutralize the temperature changes observed by the cells. Primary rat cardiomyocytes can proliferate and align reaching confluence after cyclic actuation of the LCE substrate. Furthermore, scaffolds with fully interconnected microchannels can be developed by molding polycaprolactone-based LCEs within a sacrificial foam structure. As indicated in a recent study, this scaffold does not show signs of major degradation until 15 weeks, allowing considerable time for cell growth.[70]

6. Conclusion and perspective

Compared with other stimuli-responsive materials such as hydrogels and SMPs, LCEs are especially promising due to their large-amplitude shape-shifting capability, modularity, and programmability. Fascinating examples that LCEs integrate with 4D printing have been shown as this burgeoning technology becomes attractive in academia. 4D printing of LCEs further extends the possibilities of building more sophisticated and noncontinuous complexes. In addition, 4D printing allows for the alignment of mesogens, which fundamentally supports the subsequent phase transition and shape changes, without extra steps such as rubbing and mechanical stretching. For example, DIW can realize molecular self-organization *via* the shear force within the nozzle of the syringe. Other printing methods also manage to generate structures with desired liquid crystallinity. The controllable spatial variation in the LC director will enhance the actuation complexity and find broad applications in smart actuators, biomedical devices, and the optical world.

Inspired by the wizardry of nature, smart actuators that mimic the behavior of plants and animals have been a field of increasing concern. We systematically reviewed the design, molecular alignment achieved by printing technology, and actuation of 3D-printed LCE constructs under various external stimuli, involving heat, light, electricity, humidity, and magnetic field. Secondly, the biomedical potentials of 4D-printed complexities are summarized. Owing to the peculiarity of polymer structure and stress required for inner molecule reorientation, load-bearing energy-dissipative materials are fabricated with various functionalities. Meanwhile, the mesogenic phase transition provides control over the cellular arrangement, thus employed as a dynamic substrate for cell culture. Furthermore, as LCEs combine the birefringence of low-molar-mass LCs with the mechanical properties of an elastic solid, the intriguing properties in optics are highly expected. Overall, 4D printing guides LCEs to be preciously devised and printed with as-printed state based on the requirement of customers, which qualifies LCE-based functional materials as excellent candidates for applications in advanced technologies.

Despite the aforementioned advantages and structural merits, the current research in 4D printing of LCEs still faces some challenges, especially regarding practical applications. In the future, interdisciplinary research and technological advances from diverse fields are required for 4D printing of LCEs, including a comprehensive perception of LCEs as ink materials, novel printing techniques, as well as reasonable design and modeling methodologies.

First, the extensive investigation of LC materials enables multifunctional inks for further expansion of 4D printing. As the properties of stimulus-responsive materials have a profound influence on the actuation methods, the robustness of the printed parts and the shape deforming speed, a deep understanding of the reversible phase changes that generate and relax internal stress. To initiate untethered and fully controllable shape-shifting, LCEs have been integrated with several additives, whereas these novel complexes may not be applicable to existing 3D printing methods or additional modification is required. Additionally, further investigation in the in-time feedback of the shape deformation as well as other properties is expected. So far, observable shape transformation is the main method of catching molecular reconfigurations. However, trivial change may happen without observable change in shape and mechanical properties, so that sensitive and fast characterization methods are required for future detection and implementation as *in vitro* sensors.

Second, to satisfy the rapid manufacturing of devices of multiscale architectures, 3D printing technologies with high resolution, high printing speed, and multimaterial capability have arisen huge academic curiosity. So far, only a limited number of printing techniques are suitable for 4D printing, by which common stimuli-responsive materials such as hydrogel and SMPs can be obtained with desired structures. As to LCEs, whose actuation depends on the anisotropy in molecular packaging, the printing availability is further qualified. As summarized in Table 1, the above-mentioned five species of printing methodologies account for most cases of 4D printing of LCEs. While extrusion-based DIW and FDM are mostly utilized in printing bulky devices with a slow print speed, vat polymerization presents a new possibility in microscale manufacturing, which is preferred by some biomedical applications. For example, DLP is a fast printing technology, especially when used with CLIP.[212]

Third, as the fourth dimension offers "life" to the printed parts, the manipulation of both original and transformed configuration needs to be elaborately identified. However, researchers lay most of their time and efforts on the materials and chemistries behind, with little work being done to empower the design challenges of this promising technology. Currently, self-construction structures such as self-folding container,[213] lattices,[214] and controllable Poisson's ratio,[215] which employs the basic bending and twisting, remain hot academic topics. However, unlike other smart materials, the peculiarity in the mesogenic arrangement of LCEs can induce flexible and programmable macroscopic transition with sophisticated constructs. In addition to design, a theoretical model is needed to accurately predict and optimize the shape-shifting behavior before the actual printing. For example, the finite element method (FEM) demonstrates accuracy and relevancy in modeling material behavior, enabling the modeling of stimuli-responsive behavior of LCEs. Zhang *et al.* fabricated 2D microscale kirigami structures by two-photon polymerizations and constructed proof-of-concept switching and information encryption systems.[216] By comparing simulation and experimental results, they confirmed stress distribution across the structure, which leads to geometry complexity.

4D printing has spurred and will remain a scientific interest for future studies with LCEs, while clarifying these aspects will pave the way for the development of 4D printing of LCEs. The remarkable processes in the past decades have laid a foundation and shown significant potential in smart devices, self-packaging, optics, and biomedical and biomedicine engineering. However, as a nascent field with a history of fewer than 5 years, 4D printing of LCEs calls for more efforts being paid for future advancement. In addition to the printing techniques, the proper integration and encapsulation of single LCs are of great importance for LCE-based functional devices. We envision more progress in this prospective field with the cooperation of nanotechnology, fluidic mechanics, materials science, and beyond.

Conflicts of interest

The authors have no conflicts of interest to declare.

Acknowledgements

This work was financially supported by the National Science Foundation through the University of California San Diego Materials Research Science and Engineering Center (UCSD MRSEC), grant number DMR-2011924, with additional support from the University of California San Diego start-up fund. The authors also acknowledge the support from the National Natural Science Foundation of China (No. 51973155) and the Natural Science Foundation of Tianjin (20JCYBJC00810).

References

1 Y. Forterre, J. M. Skotheim, J. Dumais and L. Mahadevan, *Nature*, 2005, **433**, 421–425.
2 J. Dumais and Y. Forterre, *Annu. Rev. Fluid Mech.*, 2012, **44**, 453–478.
3 L. M. Mäthger and R. T. Hanlon, *Cell Tissue Res.*, 2007, **329**, 179–186.
4 H. Yousuf, A. Y. Zainal, M. Alshurideh and S. A. Salloum, *Artificial Intelligence for Sustainable Development: Theory, Practice and Future Applications*, Springer, 2021, pp. 231–242.
5 C. S. X. Ng, M. W. M. Tan, C. Xu, Z. Yang, P. S. Lee and G. Z. Lum, *Adv. Mater.*, 2021, **33**, 2003558.
6 E. Sachyani Keneth, A. Kamyshny, M. Totaro, L. Beccai and S. Magdassi, *Adv. Mater.*, 2021, **33**, 2003387.
7 G. M. Whitesides, *Angew. Chem., Int. Ed.*, 2018, **57**, 4258–4273.
8 M. Cianchetti, C. Laschi, A. Menciassi and P. Dario, *Nat. Rev. Mater.*, 2018, **3**, 143–153.
9 P. Theato, B. S. Sumerlin, R. K. O'Reilly and T. H. Epps III, *Chem. Soc. Rev.*, 2013, **42**, 7055–7056.
10 Q. Zhao, H. J. Qi and T. Xie, *Prog. Polym. Sci.*, 2015, **49**, 79–120.
11 H. Meng and G. Li, *Polymer*, 2013, **54**, 2199–2221.
12 Y. Kim, H. Yuk, R. Zhao, S. A. Chester and X. Zhao, *Nature*, 2018, **558**, 274–279.
13 C. Li, Y. Jiao, X. Lv, S. Wu, C. Chen, Y. Zhang, J. Li, Y. Hu, D. Wu and J. Chu, *ACS Appl. Mater. Interfaces*, 2020, **12**, 13464–13472.
14 R. T. Shafranek, S. C. Millik, P. T. Smith, C.-U. Lee, A. J. Boydston and A. Nelson, *Prog. Polym. Sci.*, 2019, **93**, 36–67.
15 I. Willner, *Acc. Chem. Res.*, 2017, **50**, 657–658.
16 J. Bae, J.-H. Na, C. D. Santangelo and R. C. Hayward, *Polymer*, 2014, **55**, 5908–5914.
17 L. Tang, L. Wang, X. Yang, Y. Feng, Y. Li and W. Feng, *Prog. Mater. Sci.*, 2021, **115**, 100702.
18 J. Mu, C. Hou, B. Zhu, H. Wang, Y. Li and Q. Zhang, *Sci. Rep.*, 2015, **5**, 9503.
19 M. Li and J. Bae, *Polym. Chem.*, 2020, **11**, 2332–2338.
20 A. C. Daly, L. Riley, T. Segura and J. A. Burdick, *Nat. Rev. Mater.*, 2020, **5**, 20–43.
21 T. Birman and D. Seliktar, *Adv. Funct. Mater.*, 2021, **31**, 2100628.

22 C. Cui, C. Fan, Y. Wu, M. Xiao, T. Wu, D. Zhang, X. Chen, B. Liu, Z. Xu, B. Qu and W. Liu, *Adv. Mater.*, 2019, **31**, 1905761.
23 A. S. Gladman, E. A. Matsumoto, R. G. Nuzzo, L. Mahadevan and J. A. Lewis, *Nat. Mater.*, 2016, **15**, 413–418.
24 N. A. Peppas, J. Z. Hilt, A. Khademhosseini and R. Langer, *Adv. Mater.*, 2006, **18**, 1345–1360.
25 D. L. Thomsen, P. Keller, J. Naciri, R. Pink, H. Jeon, D. Shenoy and B. R. Ratna, *Macromolecules*, 2001, **34**, 5868–5875.
26 M. Camacho-Lopez, H. Finkelmann, P. Palffy-Muhoray and M. Shelley, *Nat. Mater.*, 2004, **3**, 307–310.
27 Y. Huang, H. K. Bisoyi, S. Huang, M. Wang, X.-M. Chen, Z. Liu, H. Yang and Q. Li, *Angew. Chem., Int. Ed.*, 2021, **60**, 11247–11251.
28 B. Ma, C. Xu, L. Cui, C. Zhao and H. Liu, *ACS Appl. Mater. Interfaces*, 2021, **13**, 5574–5582.
29 A. Kaiser, M. Winkler, S. Krause, H. Finkelmann and A. M. Schmidt, *J. Mater. Chem.*, 2009, **19**, 538–543.
30 K. M. Herbert, H. E. Fowler, J. M. McCracken, K. R. Schlafmann, J. A. Koch and T. J. White, *Nat. Rev. Mater.*, 2021, **7**, 23–38.
31 M. O. Saed, A. Gablier and E. M. Terentjev, *Chem. Rev.*, 2022, **122**, 4927–4945.
32 D. J. Roach, C. Yuan, X. Kuang, V. C.-F. Li, P. Blake, M. L. Romero, I. Hammel, K. Yu and H. J. Qi, *ACS Appl. Mater. Interfaces*, 2019, **11**, 19514–19521.
33 L. Wang, *Liq. Cryst.*, 2016, **43**, 2062–2078.
34 L. Wang and Q. Li, *Chem. Soc. Rev.*, 2018, **47**, 1044–1097.
35 R. Lan, J. Sun, C. Shen, R. Huang, Z. Zhang, L. Zhang, L. Wang and H. Yang, *Adv. Mater.*, 2020, **32**, 1906319.
36 Y. Sato, K. Sato and T. Uchida, *Jpn. J. Appl. Phys.*, 1992, **31**, L579.
37 M. Tabrizi, T. H. Ware and M. R. Shankar, *ACS Appl. Mater. Interfaces*, 2019, **11**, 28236–28245.
38 T. Schultz, J. Quenneville, B. Levine, A. Toniolo, T. J. Martínez, S. Lochbrunner, M. Schmitt, J. P. Shaffer, M. Z. Zgierski and A. Stolow, *J. Am. Chem. Soc.*, 2003, **125**, 8098–8099.
39 J. del Barrio and C. Sánchez-Somolinos, *Adv. Opt. Mater.*, 2019, **7**, 1900598.
40 R. Kizhakidathazhath, Y. Geng, V. S. R. Jampani, C. Charni, A. Sharma and J. P. F. Lagerwall, *Adv. Funct. Mater.*, 2020, **30**, 1909537.
41 S. W. Ula, N. A. Traugutt, R. H. Volpe, R. R. Patel, K. Yu and C. M. Yakacki, *Liq. Cryst. Rev.*, 2018, **6**, 78–107.
42 L. Hu, Y. Wan, Q. Zhang and M. J. Serpe, *Adv. Funct. Mater.*, 2020, **30**, 1903471.
43 F. Momeni, S. M. M. N. Hassani, X. Liu and J. Ni, *Mater. Des.*, 2017, **122**, 42–79.
44 X. Wang, M. Jiang, Z. Zhou, J. Gou and D. Hui, *Composites, Part B*, 2017, **110**, 442–458.
45 S. D. Gittard and R. Narayan, *Expert Rev. Med. Devices*, 2010, **7**, 343–356.
46 D. D. Gu, W. Meiners, K. Wissenbach and R. Poprawe, *Int. Mater. Rev.*, 2012, **57**, 133–164.
47 W. Gao, Y. Zhang, D. Ramanujan, K. Ramani, Y. Chen, C. B. Williams, C. C. L. Wang, Y. C. Shin, S. Zhang and P. D. Zavattieri, *Comput. Aided Des.*, 2015, **69**, 65–89.
48 S. Tibbits, *Archit. Des.*, 2014, **84**, 116–121.
49 C. P. Ambulo, J. J. Burroughs, J. M. Boothby, H. Kim, M. R. Shankar and T. H. Ware, *ACS Appl. Mater. Interfaces*, 2017, **9**, 37332–37339.
50 Y. Cheng, K. H. Chan, X.-Q. Wang, T. Ding, T. Li, X. Lu and G. W. Ho, *ACS Nano*, 2019, **13**, 13176–13184.
51 Z. Chen, D. Zhao, B. Liu, G. Nian, X. Li, J. Yin, S. Qu and W. Yang, *Adv. Funct. Mater.*, 2019, **29**, 1900971.
52 R. Lan, Y. Gao, C. Shen, R. Huang, J. Bao, Z. Zhang, Q. Wang, L. Zhang and H. Yang, *Adv. Funct. Mater.*, 2021, **31**, 2010578.
53 C. Yuan, D. J. Roach, C. K. Dunn, Q. Mu, X. Kuang, C. M. Yakacki, T. J. Wang, K. Yu and H. J. Qi, *Soft Matter*, 2017, **13**, 5558–5568.
54 A. E. Jakus, N. R. Geisendorfer, P. L. Lewis and R. N. Shah, *Acta Biomater.*, 2018, **72**, 94–109.
55 J. Chen, X. Liu, Y. Tian, W. Zhu, C. Yan, Y. Shi, L. B. Kong, H. J. Qi and K. Zhou, *Adv. Mater.*, 2021, **34**, 2102877.
56 X. Wan, L. Luo, Y. Liu and J. Leng, *Adv. Sci.*, 2020, **7**, 2001000.
57 S. Gantenbein, K. Masania, W. Woigk, J. P. W. Sesseg, T. A. Tervoort and A. R. Studart, *Nature*, 2018, **561**, 226–230.
58 O. M. Wani, H. Zeng, P. Wasylczyk and A. Priimagi, *Adv. Opt. Mater.*, 2018, **6**, 1700949.
59 N. A. Traugutt, D. Mistry, C. Luo, K. Yu, Q. Ge and C. M. Yakacki, *Adv. Mater.*, 2020, **32**, 2000797.
60 C. L. van Oosten, C. W. M. Bastiaansen and D. J. Broer, *Nat. Mater.*, 2009, **8**, 677–682.
61 Y. S. Lui, W. T. Sow, L. P. Tan, Y. Wu, Y. Lai and H. Li, *Acta Biomater.*, 2019, **92**, 19–36.
62 S. Ma, Y. Zhang, M. Wang, Y. Liang, L. Ren and L. Ren, *Sci. China: Technol. Sci.*, 2020, **63**, 532–544.
63 C. A. Spiegel, M. Hippler, A. Muenchinger, M. Bastmeyer, C. Barner-Kowollik, M. Wegener and E. Blasco, *Adv. Funct. Mater.*, 2020, **30**, 1907615.
64 I. Apsite, A. Biswas, Y. Li and L. Ionov, *Adv. Funct. Mater.*, 2020, **30**, 1908028.
65 M. Del Pozo, J. A. Sol, A. P. Schenning and M. G. Debije, *Adv. Mater.*, 2021, 2104390.
66 Y. C. Cheng, H. C. Lu, X. Lee, H. Zeng and A. Priimagi, *Adv. Mater.*, 2020, **32**, 1906233.
67 A. Kotikian, C. McMahan, E. C. Davidson, J. M. Muhammad, R. D. Weeks, C. Daraio and J. A. Lewis, *Sci. Robot.*, 2019, **4**, eaax7044.
68 X. Lu, C. P. Ambulo, S. Wang, L. K. Rivera-Tarazona, H. Kim, K. Searles and T. H. Ware, *Angew. Chem., Int. Ed.*, 2021, **60**, 5536–5543.
69 M. Lopez-Valdeolivas, D. Liu, D. J. Broer and C. Sanchez-Somolinos, *Macromol. Rapid Commun.*, 2018, **39**, 1700710.
70 T. Mori, R. Cukelj, M. E. Prévôt, S. Ustunel, A. Story, Y. Gao, K. Diabre, J. A. McDonough, E. J. Freeman, E. Hegmann and R. J. Clements, *Macromol. Rapid Commun.*, 2020, **41**, 1900585.

71 R. H. Volpe, D. Mistry, V. V. Patel, R. R. Patel and C. M. Yakacki, *Adv. Healthc. Mater.*, 2020, **9**, 1901136.
72 L. Wang and Q. Li, *Adv. Funct. Mater.*, 2016, **26**, 10–28.
73 Y. Yang, L. Wang, H. Yang and Q. Li, *Small Sci.*, 2021, **1**, 2100007.
74 Z. Zheng, Y. Li, H. K. Bisoyi, L. Wang, T. J. Bunning and Q. Li, *Nature*, 2016, **531**, 352–356.
75 P. De Gennes, *Seances Acad. Sci. B*, 1975, **281**, 101.
76 P. De Gennes and J. Prost, *The physics of liquid crystals*, Oxford University Press, 1993.
77 C. Noel and P. Navard, *Prog. Polym. Sci.*, 1991, **16**, 55–110.
78 A. Al-Dujaili, A. Jenkins and D. Walton, *J. Polym. Sci. A: Polym. Chem.*, 1984, **22**, 3129–3133.
79 J. L. White and J. E. Spruiell, *Polym. Eng. Sci.*, 1983, **23**, 247–256.
80 M. Deutsch, *Phys. Rev. A*, 1991, **44**, 8264.
81 J. Planer, *Ann. Chem. Pharm.*, 1861, **118**, 25–27.
82 X. Liang, C. Guo, M. Chen, S. Guo, L. Zhang, F. Li, S. Guo and H. Yang, *Nanoscale Horiz.*, 2017, **2**, 319–325.
83 C. Yang, B. Wu, J. Ruan, P. Zhao, L. Chen, D. Chen and F. Ye, *Adv. Mater.*, 2021, **33**, 2006361.
84 M. Sheng, L. Zhang, S. Jiang, L. Yang, F. Zaaboul and S. Fu, *ACS Appl. Mater. Interfaces*, 2021, **13**, 13586–13595.
85 M. Sheng, L. Zhang, J. L. West and S. Fu, *ACS Appl. Mater. Interfaces*, 2020, **12**, 29728–29736.
86 M. Song, J. Seo, H. Kim and Y. Kim, *Sci. Rep.*, 2017, **7**, 1–11.
87 X. Liang, S. Guo, M. Chen, C. Li, Q. Wang, C. Zou, C. Zhang, L. Zhang, S. Guo and H. Yang, *Mater. Horiz.*, 2017, **4**, 878–884.
88 H. Ma, L. Zhou, C. Han, C. Zhang and L. Zhang, *Liq. Cryst.*, 2019, **46**, 138–144.
89 C. Ohm, M. Brehmer and R. Zentel, *Adv. Mater.*, 2010, **22**, 3366–3387.
90 F. Brömmel, D. Kramer and H. Finkelmann, in *Liquid Crystal Elastomers: Materials and Applications*, ed. W. H. de Jeu, Springer Berlin Heidelberg, Berlin, Heidelberg, 2012, pp. 1–48.
91 T. J. White and D. J. Broer, *Nat. Mater.*, 2015, **14**, 1087–1098.
92 P. Beyer, E. M. Terentjev and R. Zentel, *Macromol. Rapid Commun.*, 2007, **28**, 1485–1490.
93 A. Azoug, V. Vasconcellos, J. Dooling, M. Saed, C. Yakacki and T. Nguyen, *Polymer*, 2016, **98**, 165–171.
94 E. M. Terentjev, *J. Phys.: Condens. Matter*, 1999, **11**, 239–257.
95 J. Kupfer and H. Finkelmann, *Macromol. Rapid Commun.*, 1991, **12**, 717–726.
96 G. H. F. Bergmann, H. Finkelmann, V. Percec and M. Y. Zhao, *Macromol. Rapid Commun.*, 1997, **18**, 353–360.
97 K. Urayama, *Macromolecules*, 2007, **40**, 2277–2288.
98 K. Kishore, *Polymer*, 1995, **36**, 1903–1910.
99 J. A. Johnson, M. G. Finn, J. T. Koberstein and N. J. Turro, *Macromol. Rapid Commun.*, 2008, **29**, 1052–1072.
100 J. Lub, D. J. Broer and N. vandenBroek, *Liebigs Ann.*, 1997, 2281–2288.
101 H. Yang, A. Buguin, J.-M. Taulemesse, K. Kaneko, S. Mery, A. Bergeret and P. Keller, *J. Am. Chem. Soc.*, 2009, **131**, 15000–15004.
102 Z. Wen, K. Yang and J.-M. Raquez, *Molecules*, 2020, **25**, 1241.
103 A. Kotikian, R. L. Truby, J. W. Boley, T. J. White and J. A. Lewis, *Adv. Mater.*, 2018, **30**, 1706164.
104 M. O. Saed, C. P. Ambulo, H. Kim, R. De, V. Raval, K. Searles, D. A. Siddiqui, J. M. O. Cue, M. C. Stefan, M. R. Shankar and T. H. Ware, *Adv. Funct. Mater.*, 2019, **29**, 1806412.
105 C. Yakacki, M. Saed, D. Nair, T. Gong, S. Reed and C. Bowman, *RSC Adv.*, 2015, **5**, 18997–19001.
106 T. H. Ware, M. E. McConney, J. J. Wie, V. P. Tondiglia and T. J. White, *Science*, 2015, **347**, 982–984.
107 L. Ren, B. Li, Y. He, Z. Song, X. Zhou, Q. Liu and L. Ren, *ACS Appl. Mater. Interfaces*, 2020, **12**, 15562–15572.
108 D. Montarnal, M. Capelot, F. Tournilhac and L. Leibler, *Science*, 2011, **334**, 965–968.
109 C. J. Kloxin and C. N. Bowman, *Chem. Soc. Rev.*, 2013, **42**, 7161–7173.
110 T. H. Ware and T. J. White, *Polym. Chem.*, 2015, **6**, 4835–4844.
111 Z. Pei, Y. Yang, Q. Chen, E. M. Terentjev, Y. Wei and Y. Ji, *Nat. Mater.*, 2014, **13**, 36–41.
112 M. O. Saed, A. Gablier and E. M. Terentejv, *Adv. Funct. Mater.*, 2020, **30**, 1906458.
113 Z. Wen, M. K. McBride, X. Zhang, X. Han, A. M. Martinez, R. Shao, C. Zhu, R. Visvanathan, N. A. Clark, Y. Wang, K. Yang and C. N. Bowman, *Macromolecules*, 2018, **51**, 5812–5819.
114 Y. Li, Y. Zhang, O. Rios, J. K. Keum and M. R. Kessler, *RSC Adv.*, 2017, **7**, 37248–37254.
115 Y. Li, Y. Zhang, O. Rios, J. K. Keum and M. R. Kessler, *Soft Matter*, 2017, **13**, 5021–5027.
116 Z. Wang, H. Tian, Q. He and S. Cai, *ACS Appl. Mater. Interfaces*, 2017, **9**, 33119–33128.
117 E. C. Davidson, A. Kotikian, S. Li, J. Aizenberg and J. A. Lewis, *Adv. Mater.*, 2020, **32**, 1905682.
118 M. K. McBride, M. Hendrikx, D. Liu, B. T. Worrell, D. J. Broer and C. N. Bowman, *Adv. Mater.*, 2017, **29**, 1606509.
119 M. K. McBride, A. M. Martinez, L. Cox, M. Alim, K. Childress, M. Beiswinger, M. Podgorski, B. T. Worrell, J. Killgore and C. N. Bowman, *Sci. Adv.*, 2018, **4**, aat4634.
120 L. Chen, H. Bisoyi, Y. Huang, S. Huang, M. Wang, H. Yang and Q. Li, *Angew. Chem., Int. Ed.*, 2021, **60**, 16394–16398.
121 H. Ringsdorf and R. Zentel, *Macromol. Chem. Phys.*, 1982, **183**, 1245–1256.
122 Z. S. Davidson, H. Shahsavan, A. Aghakhani, Y. Guo, L. Hines, Y. Xia, S. Yang and M. Sitti, *Sci. Adv.*, 2019, **5**, eaay0855.
123 J. Zhang, Y. Guo, W. Hu, R. H. Soon, Z. S. Davidson and M. Sitti, *Adv. Mater.*, 2021, **33**, 2006191.
124 C. Ahn, X. Liang and S. Cai, *Extreme Mech. Lett.*, 2015, **5**, 30–36.
125 C. M. Spillmann, B. R. Ratna and J. Naciri, *Appl. Phys. Lett.*, 2007, **90**, 021911.
126 S.-J. Ge, T.-P. Zhao, M. Wang, L.-L. Deng, B.-P. Lin, X.-Q. Zhang, Y. Sun, H. Yang and E.-Q. Chen, *Soft Matter*, 2017, **13**, 5463–5468.

127 I. Ibrahim and W. Haase, *J. Phys. Colloques*, 1979, **40**, 164–168.
128 A. Komp, J. Rühe and H. Finkelmann, *Macromol. Rapid Commun.*, 2005, **26**, 813–818.
129 S. Kumar, J.-H. Kim and Y. Shi, *Phys. Rev. Lett.*, 2005, **94**, 077803.
130 Y. Guo, M. Jiang, C. Peng, K. Sun, O. Yaroshchuk, O. Lavrentovich and Q. H. Wei, *Adv. Mater.*, 2016, **28**, 2353–2358.
131 K. Ichimura, *Chem. Rev.*, 2000, **100**, 1847–1874.
132 S. k. Ahn, T. H. Ware, K. M. Lee, V. P. Tondiglia and T. J. White, *Adv. Funct. Mater.*, 2016, **26**, 5819–5826.
133 S.-C. Jeng and S.-J. Hwang, *High performance polymers-polyimides based-from chemistry to applications*, 2012.
134 L. Wang, A. M. Urbas and Q. Li, *Adv. Mater.*, 2020, **32**, 1801335.
135 M. Zeng, D. King, D. Huang, C. Do, L. Wang, M. Chen, S. Lei, P. Lin, Y. Chen and Z. Cheng, *Proc. Natl. Acad. Sci. U. S. A.*, 2019, **116**, 18322–18327.
136 F. C. Frank, *Discuss. Faraday Soc.*, 1958, **25**, 19–28.
137 Y. Xia, G. Cedillo-Servin, R. D. Kamien and S. Yang, *Adv. Mater.*, 2016, **28**, 9637–9643.
138 L. M. Cox, A. M. Martinez, A. K. Blevins, N. Sowan, Y. Ding and C. N. Bowman, *Nano Today*, 2020, **31**, 100838.
139 L. Chen, Y. Dong, C. Y. Tang, L. Zhong, W. C. Law, G. C. P. Tsui, Y. Yang and X. Xie, *ACS Appl. Mater. Interfaces*, 2019, **11**, 19541–19553.
140 Y. Guo, H. Shahsavan and M. Sitti, *Adv. Mater.*, 2020, **32**, 2002753.
141 X. Kuang, D. J. Roach, J. Wu, C. M. Hamel, Z. Ding, T. Wang, M. L. Dunn and H. J. Qi, *Adv. Funct. Mater.*, 2019, **29**, 1805290.
142 C. Zhang, X. Lu, G. Fei, Z. Wang, H. Xia and Y. Zhao, *ACS Appl. Mater. Interfaces*, 2019, **11**, 44774–44782.
143 S. Li, H. Bai, Z. Liu, X. Zhang, C. Huang, L. W. Wiesner, M. Silberstein and R. F. Shepherd, *Sci. Adv.*, 2021, **7**, eabg3677.
144 H. Zeng, P. Wasylczyk, G. Cerretti, D. Martella, C. Parmeggiani and D. S. Wiersma, *Appl. Phys. Lett.*, 2015, **106**, 111902.
145 P. Calvert, *Chem. Mater.*, 2001, **13**, 3299–3305.
146 D. J. Roach, X. Kuang, C. Yuan, K. Chen and H. J. Qi, *Smart Mater. Struct.*, 2018, **27**, 125011.
147 M. Barnes, S. M. Sajadi, S. Parekh, M. M. Rahman, P. M. Ajayan and R. Verduzco, *ACS Appl. Mater. Interfaces*, 2020, **12**, 28692–28699.
148 Z. Wang, Z. Wang, Y. Zheng, Q. He, Y. Wang and S. Cai, *Sci. Adv.*, 2020, **6**, eabc0034.
149 Z. Ding, C. Yuan, X. Peng, T. Wang, H. J. Qi and M. L. Dunn, *Sci. Adv.*, 2017, **3**, e160289.
150 C. P. Ambulo, M. J. Ford, K. Searles, C. Majidi and T. H. Ware, *ACS Appl. Mater. Interfaces*, 2021, **13**, 12805–12813.
151 A. K. Sood, R. K. Ohdar and S. S. Mahapatra, *Mater. Des.*, 2010, **31**, 287–295.
152 W. Li, L. S. Mille, J. A. Robledo, T. Uribe, V. Huerta and Y. S. Zhang, *Adv. Healthc. Mater.*, 2020, **9**, 2000156.
153 B. Levrand and A. Herrmann, *Photochem. Photobiol.*, 2002, **1**, 907–919.
154 S. Nocentini, D. Martella, C. Parmeggiani, S. Zanotto and D. S. Wiersma, *Adv. Opt. Mater.*, 2018, **6**, 1800167.
155 H. Zeng, P. Wasylczyk, C. Parmeggiani, D. Martella, M. Burresi and D. S. Wiersma, *Adv. Mater.*, 2015, **27**, 3883–3887.
156 M. Rumi and J. W. Perry, *Adv. Opt. Photon.*, 2010, **2**, 451–518.
157 Y. Guo, J. Zhang, W. Hu, M. T. A. Khan and M. Sitti, *Nat. Commun.*, 2021, **12**, 1–9.
158 Q. Mu, L. Wang, C. K. Dunn, X. Kuang, F. Duan, Z. Zhang, H. J. Qi and T. Wang, *Addit. Manuf.*, 2017, **18**, 74–83.
159 M. Singh, H. M. Haverinen, P. Dhagat and G. E. Jabbour, *Adv. Mater.*, 2010, **22**, 673–685.
160 F. Zhai, Y. Feng, Z. Li, Y. Xie, J. Ge, H. Wang, W. Qiu and W. Feng, *Matter*, 2021, **4**, 3313–3326.
161 Z. Wang and S. Cai, *J. Mater. Chem. B*, 2020, **8**, 6610–6623.
162 Y. Chen, J. Yang, X. Zhang, Y. Feng, H. Zeng, L. Wang and W. Feng, *Mater. Horiz.*, 2021, **8**, 728–757.
163 J. Yang, X. Zhang, X. Zhang, L. Wang, W. Feng and Q. Li, *Adv. Mater.*, 2021, **33**, 2004754.
164 J. P. F. Lagerwall and G. Scalia, *J. Mater. Chem.*, 2008, **18**, 2890–2898.
165 P. Kumar, U. N. Maiti, K. E. Lee and S. O. Kim, *Carbon*, 2014, **80**, 453–461.
166 M. Yang, Y. Xu, X. Zhang, H. K. Bisoyi, P. Xue, Y. Yang, X. Yang, C. Valenzuela, Y. Chen and L. Wang, *Adv. Funct. Mater.*, 2022, 2201884.
167 M. Baginski, M. Tupikowska, G. Gonzalez-Rubio, M. Wojcik and W. Lewandowski, *Adv. Mater.*, 2020, **32**, 1904581.
168 X. Yang, Y. Chen, X. Zhang, P. Xue, P. Lv, Y. Yang, L. Wang and W. Feng, *Nano Today*, 2022, **43**, 101419.
169 T. Ube, K. Kawasaki and T. Ikeda, *Adv. Mater.*, 2016, **28**, 8212–8217.
170 M. Wang, B.-P. Lin and H. Yang, *Nat. Commun.*, 2016, **7**, 13981.
171 D. A. Paterson, J. Xiang, G. Singh, R. Walker, D. A. M. Agra-Kooijman, A. Martinez-Felipe, M. Gao, J. M. Storey, S. Kumar and O. D. Lavrentovich, *J. Am. Chem. Soc.*, 2016, **138**, 5283–5289.
172 S. H. Söntjens, R. P. Sijbesma, M. H. van Genderen and E. Meijer, *J. Am. Chem. Soc.*, 2000, **122**, 7487–7493.
173 S. Kim, F. Qiu, S. Kim, A. Ghanbari, C. Moon, L. Zhang, B. J. Nelson and H. Choi, *Adv. Mater.*, 2013, **25**, 5863–5868.
174 F. Qiu, R. Mhanna, L. Zhang, Y. Ding, S. Fujita and B. J. Nelson, *Sens. Actuators, B*, 2014, **196**, 676–681.
175 R. A. Freitas Jr, *Int. J. Surg.*, 2005, **3**, 243–246.
176 H. Zeng, P. Wasylczyk, C. Parmeggiani, D. Martella, M. Burresi and D. S. Wiersma, *Adv. Mater.*, 2015, **27**, 3883–3887.
177 M. Chambers, H. Finkelmann, M. Remškar, A. Sánchez-Ferrer, B. Zalar and S. Žumer, *J. Mater. Chem.*, 2009, **19**, 1524–1531.
178 H. Kim, J. A. Lee, C. P. Ambulo, H. B. Lee, S. H. Kim, V. V. Naik, C. S. Haines, A. E. Aliev, R. Ovalle-Robles and R. H. Baughman, *Adv. Funct. Mater.*, 2019, **29**, 1905063.

179 J. Liu, Y. Gao, H. Wang, R. Poling-Skutvik, C. O. Osuji and S. Yang, *Adv. Intell. Syst.*, 2020, **2**, 1900163.
180 A. Agrawal, H. Chen, H. Kim, B. Zhu, O. Adetiba, A. Miranda, A. Cristian Chipara, P. M. Ajayan, J. G. Jacot and R. Verduzco, *ACS Macro Lett.*, 2016, **5**, 1386–1390.
181 S. Chen, H.-Z. Wang, R.-Q. Zhao, W. Rao and J. Liu, *Matter*, 2020, **2**, 1446–1480.
182 W. Zhang, J. Chen, X. Li and Y. Lu, *Small*, 2020, **16**, e2004190.
183 J.-Y. Gao, S. Chen, T.-Y. Liu, J. Ye and J. Liu, *Mater. Today*, 2021, **49**, 201–230.
184 P. Lv, X. Yang, H. K. Bisoyi, H. Zeng, X. Zhang, Y. Chen, P. Xue, S. Shi, A. Priimagi and L. Wang, *Mater. Horiz.*, 2021, **8**, 2475–2484.
185 A. Kotikian, J. M. Morales, A. Lu, J. Mueller, Z. S. Davidson, J. W. Boley and J. A. Lewis, *Adv. Mater.*, 2021, **33**, 2101814.
186 J. M. Boothby and T. H. Ware, *Soft Matter*, 2017, **13**, 4349–4356.
187 K. D. Harris, C. W. Bastiaansen, J. Lub and D. J. Broer, *Nano Lett.*, 2005, **5**, 1857–1860.
188 R. C. P. Verpaalen, M. G. Debije, C. W. M. Bastiaansen, H. Halilović, T. A. P. Engels and A. P. H. J. Schenning, *J. Mater. Chem. A*, 2018, **6**, 17724–17729.
189 R. C. P. Verpaalen, A. E. J. Souren, M. G. Debije, T. A. P. Engels, C. W. M. Bastiaansen and A. P. H. J. Schenning, *Soft Matter*, 2020, **16**, 2753–2759.
190 O. M. Wani, R. Verpaalen, H. Zeng, A. Priimagi and A. Schenning, *Adv. Mater.*, 2019, **31**, 1805985.
191 Y. Liu, B. Xu, S. Sun, J. Wei, L. Wu and Y. Yu, *Adv. Mater.*, 2017, **29**, 1604792.
192 R. Lan, J. Sun, C. Shen, R. Huang, L. Zhang and H. Yang, *Adv. Funct. Mater.*, 2019, **29**, 1900013.
193 K. Kim, Y. Guo, J. Bae, S. Choi, H. Y. Song, S. Park, K. Hyun and S. K. Ahn, *Small*, 2021, **17**, 2100910.
194 W. Shi, J. Huang, R. Fang and M. Liu, *ACS Appl. Mater. Interfaces*, 2020, **12**, 5177–5194.
195 J. Zhang, Y. Guo, W. Hu and M. Sitti, *Adv. Mater.*, 2021, **33**, 2100336.
196 L. Phan, W. G. Walkup IV, D. D. Ordinario, E. Karshalev, J. M. Jocson, A. M. Burke and A. A. Gorodetsky, *Adv. Mater.*, 2013, **25**, 5621–5625.
197 L. Zhang, L. Wang, U. S. Hiremath, H. K. Bisoyi, G. G. Nair, C. V. Yelamaggad, A. M. Urbas, T. J. Bunning and Q. Li, *Adv. Mater.*, 2017, **29**, 1700676.
198 L. Wang, D. Chen, K. G. Gutierrez-Cuevas, H. K. Bisoyi, J. Fan, R. S. Zola, G. Li, A. M. Urbas, T. J. Bunning and D. A. Weitz, *Mater. Horiz.*, 2017, **4**, 1190–1195.
199 L. Wang, H. K. Bisoyi, Z. Zheng, K. G. Gutierrez-Cuevas, G. Singh, S. Kumar, T. J. Bunning and Q. Li, *Mater. Today*, 2017, **20**, 230–237.
200 L. Wang, H. Dong, Y. Li, R. Liu, Y. F. Wang, H. K. Bisoyi, L. D. Sun, C. H. Yan and Q. Li, *Adv. Mater.*, 2015, **27**, 2065–2069.
201 M. Moirangthem and A. Schenning, *ACS Appl. Mater. Interfaces*, 2018, **10**, 4168–4172.
202 J. Yang, W. Zhao, Z. Yang, W. He, J. Wang, T. Ikeda and L. Jiang, *J. Mater. Chem. C*, 2019, **7**, 13764–13769.
203 Y. Yang, X. Zhang, Y. Chen, X. Yang, J. Ma, J. Wang, L. Wang and W. Feng, *ACS Appl. Mater. Interfaces*, 2021, **13**, 41102–41111.
204 J. A. Sol, H. Sentjens, L. Yang, N. Grossiord, A. P. Schenning and M. G. Debije, *Adv. Mater.*, 2021, **33**, 2103309.
205 W. Zhao, L. Liu, F. Zhang, J. Leng and Y. Liu, *Mater. Sci. Eng. C: Mater. Biol. Appl.*, 2019, **97**, 864–883.
206 A. S. Hoffman, *Adv. Drug Delivery Rev.*, 2012, **64**, 18–23.
207 C. P. Ambulo, S. Tasmim, S. Wang, M. K. Abdelrahman, P. E. Zimmern and T. H. Ware, *J. Appl. Phys.*, 2020, **128**, 140901.
208 R. K. Shaha, D. R. Merkel, M. P. Anderson, E. J. Devereaux, R. R. Patel, A. H. Torbati, N. Willett, C. M. Yakacki and C. P. Frick, *J. Mech. Behav. Biomed. Mater.*, 2020, **107**, 103757.
209 D. Mistry, N. A. Traugutt, B. Sanborn, R. H. Volpe, L. S. Chatham, R. Zhou, B. Song, K. Yu, K. N. Long and C. M. Yakacki, *Nat. Commun.*, 2021, **12**, 6677.
210 C. Luo, C. Chung, N. A. Traugutt, C. M. Yakacki, K. N. Long and K. Yu, *ACS Appl. Mater. Interfaces*, 2021, **13**, 12698–12708.
211 S.-Y. Jeon, B. Shen, N. A. Traugutt, Z. Zhu, L. Fang, C. M. Yakacki, T. D. Nguyen and S. H. Kang, *Adv. Mater.*, 2022, **34**, 2200272.
212 J. R. Tumbleston, D. Shirvanyants, N. Ermoshkin, R. Janusziewicz, A. R. Johnson, D. Kelly, K. Chen, R. Pinschmidt, J. P. Rolland, A. Ermoshkin, E. T. Samulski and J. M. DeSimone, *Science*, 2015, **347**, 1349–1352.
213 Q. Ge, H. J. Qi and M. L. Dunn, *Appl. Phys. Lett.*, 2013, **103**, 131901.
214 Q. Zhang, K. Zhang and G. Hu, *Sci. Rep.*, 2016, **6**, 22431.
215 J. Wu, Z. Zhao, X. Kuang, C. M. Hamel, D. Fang and H. J. Qi, *Multifunct. Mater.*, 2018, **1**, 015002.
216 M. Zhang, H. Shahsavan, Y. Guo, A. Pena-Francesch, Y. Zhang and M. Sitti, *Adv. Mater.*, 2021, **33**, 2008605.